Tectonics®

RESEARCH ARTICLE
10.1029/2021TC006706

Key Points:

- Normal faults, strike-slip faults and monoclines formed in west-northwest- or northeast-trending structural zones during flexural extension
- Varying proportions of normal and strike slip faults and extension directions indicate extension was focused over basement weaknesses
- Faults that record north-south shortening overprint the structural zones, with incipient inversion and fluid flux focused at block corners

Supporting Information:

Supporting Information may be found in the online version of this article.

Correspondence to:

M. R. Hudson,
mhudson@usgs.gov

Citation:

Hudson, M. R., & Turner, K. J. (2022). Late Paleozoic flexural extension and overprinting shortening in the southern Ozark dome, Arkansas, USA: Evolving fault kinematics in the foreland of the Ouachita orogen. *Tectonics*, *41*, e2021TC006706. https://doi.org/10.1029/2021TC006706

Received 6 JAN 2021
Accepted 13 MAY 2022

Author Contributions:

Conceptualization: Mark R. Hudson
Data curation: Mark R. Hudson, Kenzie J. Turner
Formal analysis: Mark R. Hudson, Kenzie J. Turner
Funding acquisition: Mark R. Hudson
Investigation: Mark R. Hudson, Kenzie J. Turner
Methodology: Mark R. Hudson, Kenzie J. Turner

Late Paleozoic Flexural Extension and Overprinting Shortening in the Southern Ozark Dome, Arkansas, USA: Evolving Fault Kinematics in the Foreland of the Ouachita Orogen

Mark R. Hudson[1] **and Kenzie J. Turner**[1]

[1]U.S. Geological Survey, Denver, CO, USA

Abstract Faults and folds on the southern flank of the Ozark dome in northern Arkansas, USA, record flexural extension in a foreland area followed by shortening in response to the late Paleozoic Ouachita orogeny. Map-scale structures and an analysis of fault-slip data collected systematically during geologic mapping demonstrate that most deformation in the area accommodated north-south extension as the southern margin of Laurentia was flexed beneath the thrust load of the Ouachita belt, probably during Middle Pennsylvanian. Extension was concentrated in northeast- and west-northwest-trending structural zones having sets of discontinuous, often en echelon normal and strike-slip faults and associated monoclinal folds. Reactivation of basement weaknesses that underlie these zones is indicated by their close match to oblique-rift models in which both the proportions of normal and strike-slip faulting and the internal extension directions vary with orientation of the zones. Subsequent propagation of north-south Ouachita shortening into the foreland formed small-offset strike-slip and sparse reverse faults that overprinted older extensional structures. Strike-slip faults were concentrated in reactivated northeast-trending structural zones. In two areas, reverse faults and local anticlines were developed in the footwalls of older normal faults, both near intersections of northeast- and west-northwest-trending structural zones. These are interpreted as areas of incipient inversion due to compressional stress concentrations at fault-block corners. Spatial overlap of areas of north-south shortening and fluid flux marked by silicification or lead-zinc mineralization indicates that regional fluid flow of brines was coeval with and may have enhanced inversion during Late Pennsylvanian to early Permian.

1. Introduction

Foreland regions of continents can record the directions and succession of deformation episodes driven by plate margin orogeny (Cox, 2009; Hancock, 1985; Hancock & Bevan, 1987) and forelands may retain a valuable record of the tectonic history if preservation of older orogens is incomplete due to subsequent rifting or burial by younger rocks (Denison, 1989; Flawn et al., 1961; Thomas, 1989). Understanding the nature and history of foreland structures is also important because of their potential influence on syntectonic sedimentation (DeCelles & Giles, 1996; Houseknecht, 1986; Lawton et al., 2021; Thomas et al., 2021) or the paths of fluids driven from orogenic belts (Bethke & Marshak, 1990; Gavin et al., 1993; Oliver, 1986). However, because deformation recorded in foreland strata may be preferentially concentrated above older basement faults, shear zones, or steeply dipping contacts that act as crustal weaknesses (Marshak & Paulsen, 1996; Thomas, 2004), care should be taken to assess whether paleostress or paleostrain directions in local deformed zones were deflected relative to regional directions.

The late Paleozoic Ouachita orogenic belt formed along the southern margin of Laurentia during the progressive east to west suturing with Gondwana and its marginal terranes from Late Mississippian through the early Permian (Dickinson & Lawton, 2003; Viele & Thomas, 1989; Wickham et al., 1976). Although much of the Ouachita orogenic belt is now buried beneath younger Gulf Coast sediments (Flawn et al., 1961; Thomas, 1989), a transect from the accretionary Ouachita fold and thrust belt through the Arkoma foreland basin (Arbenz, 2008; Sutherland, 1988) and into the foreland uplift of the Ozark dome (Croneis, 1930) is well exposed in western Arkansas (Figure 1). This study makes use of geologic mapping conducted in good exposures of the Buffalo River drainage to describe the characteristics of foreland faults and folds and to present a fault-slip analysis for the southern flank of the Ozark dome. It documents episodes of flexural extension and subsequent incipient inversion that can be linked to the Ouachita orogeny as it encroached from the south. The study also highlights the

Project Administration: Mark R. Hudson
Supervision: Mark R. Hudson
Visualization: Mark R. Hudson
Writing – original draft: Mark R. Hudson
Writing – review & editing: Mark R. Hudson, Kenzie J. Turner

probable importance of preexisting basement weaknesses that influenced the location and character of foreland deformation and investigates the temporal relations between the deformation episodes and regional paleofluid flow driven from the Ouachita orogen.

2. Geologic Setting

The Ozark dome (Figure 1) is one of several basement highs that experienced uplift inboard from late Paleozoic foreland basins that developed at the margins of Laurentia in response to the Ouachita and Alleghanian orogenies (Marshak et al., 2017; Quinlan & Beaumont, 1984; Thomas, 1989). The crest of the Ozark dome trends west-southwest across southern Missouri (Siebenthal, 1915), exposing Mesoproterozoic crystalline basement in the deeply eroded St. Francois Mountains. Southward from the crest, progressively younger Cambrian-Ordovician, Lower to Middle Mississippian, and Upper Mississippian-Middle Pennsylvanian stratigraphic intervals are exposed beneath physiographic plateaus of the Salem, Springfield, and Boston Mountains provinces, respectively. Pennsylvanian strata of the Boston Mountains dip gently southward and are downfaulted into the Arkoma foreland basin, with the large Mulberry normal fault taken as the boundary between the provinces (Arbenz, 1989). The Arkoma basin was filled with flysch and broken by contemporaneous normal faulting (Buchanan & Johnson, 1968; Houseknecht, 1986) that began in the Middle Pennsylvanian (Figure 2, Atokan stage) in response to crustal flexure caused by thrusting of deep-water, preorogenic Cambrian through Lower Mississippian strata onto the continental shelf as part of the accretionary Ouachita fold and thrust belt (Viele & Thomas, 1989). Continued northward propagation of Ouachita shortening incorporated the foreland basin flysch deposits into frontal thrust plates and folds above blind thrusts. Folded Desmoinesian strata are the youngest preserved deposits within the Arkoma basin in western Arkansas, although shortening probably continued into the Late Pennsylvanian to early Permian as Pangea was assembled (Viele & Thomas, 1989). Compression of the Arkoma basin and growth of topographic head in the Ouachita fold and thrust belt drove regional-scale fluid flow northward into the foreland areas (Bethke & Marshak, 1990; Clendenin & Duane, 1990; Lewchuk & Symons, 1995; Appold & Nunn, 2005), with fluid inclusions recording passage of warm basinal brines through sedimentary rocks of the Ozark dome (Leach & Rowan, 1996). Late Pennsylvanian to early Permian ages from paleomagnetic (Lewchuk & Symons, 1995; Pan et al., 1990) and isotopic studies (Brannon et al., 1996) of Mississippi-Valley-type mineralization support the linkage of regional fluid flow to the Ouachita orogeny (Leach et al., 2001).

The study area is located in northwestern Arkansas on the southern flank of the Ozark dome, about 50 km north of the northern boundary of the Arkoma basin and about 100 km north of the northernmost through-going frontal Ross Creek thrust fault of the Ouachita fold and thrust belt (Figure 1). The area is centered on the watershed for the Buffalo River (Figure 3) where valley incision has exposed a 500-m-thick sequence of gently dipping Paleozoic sedimentary strata as well as a series of spaced faults and folds that have been documented in recent 1:24,000-scale geologic maps (Chandler & Ausbrooks, 2003; Chandler & Ausbrooks, 2015a, 2015b, 2015c; Hudson & Murray, 2003; Hudson & Turner, 2007; Hudson & Turner, 2014a; Hudson & Turner, 2016; Turner & Hudson, 2018). The oldest exposed rocks are Ordovician carbonates and sandstones, locally overlain by Silurian limestones where preserved beneath a regional unconformity at the base of the Mississippian section. Lower to Middle Mississippian Boone Formation is a widely exposed 120-m-thick unit of cherty limestone whose contacts provide key markers for structural control in the area. Intervals of sandstone, shale and less common limestone make up Upper Mississippian (Chesterian) through Lower to Middle Pennsylvanian (Morrowan and Atokan) stratigraphic intervals that cap the study area. The prominent cliff-forming middle Bloyd sandstone of the Bloyd Formation (Morrowan) is another important horizon for structural control in the area.

3. Methods

Data used to define and characterize faults and folds in the study area were gathered at numerous field sites occupied during geologic mapping for areas published by the U.S. Geological Survey and from targeted inspections of structural features in areas mapped by the Arkansas Geological Survey (Figure 3b).

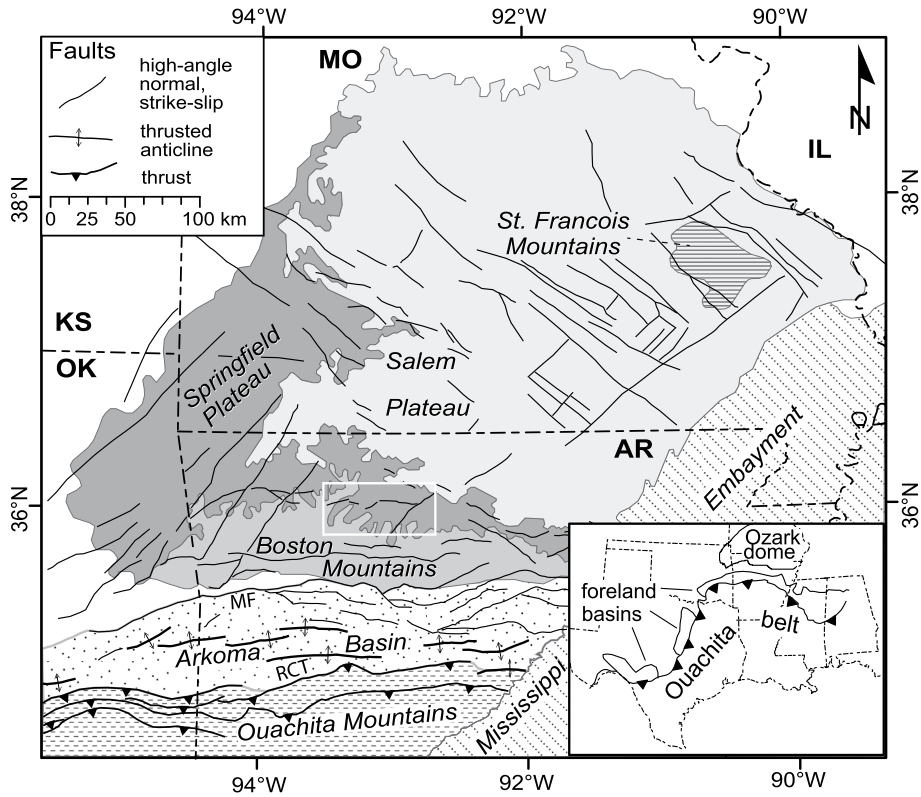

Figure 1. Physiographic provinces and major faults showing regional geologic setting for the Ouachita fold and thrust belt, Arkoma basin, and Ozark dome. White box is the southern Ozarks study area. Inset on lower right shows setting within larger Ouachita orogenic belt. Named faults are MF – Mulberry fault and RCT – Ross Creek thrust. Illustration combined from Bradley and Kidd (1991), Cox (2009), Haley et al. (1993), Miser (1954), and Starbuck (2017).

3.1. Identification and Assessment of Map-Scale and Mesoscale Structures

Map-scale faults that were identified and traced through the study area mostly have lengths of greater than a kilometer, throws greater than 15 m, and either northeast or west-northwest to west strikes, often with en echelon arrangements (Figure 3). Tracing of the map-scale faults was aided by outcrop-scale exposures of the faults and their damage zones, with fault rocks displaying different characteristics in different lithologies (Figure 4). The Mississippian Boone Formation developed fault breccias of angular chert clasts in limestone gouge (Figure 4a). Dense networks of deformation bands (Aydin & Johnson, 1978; Davis, 1999) were developed in damage zones of faults cutting porous sandstones of the Ordovician Everton Formation and St. Peter Sandstone (Figure 4b) or some areas of the middle Bloyd sandstone of the Pennsylvanian Bloyd Formation. Other faults in sandstones and siltstones have planes that preserve frictional wear striae (Figure 4c) that may contain intersecting Riedel or tension fractures.

Mesoscale structures are dominated by small-offset faults, most having offsets from millimeters to less than 2 m (Figure 4). The field practice during geologic mapping was to note any indication of faulting no matter the size. Because field sites were occupied across the area, the absence of observations of even mesoscale faults in large parts of the study area demonstrates that fault growth was spatially concentrated within certain zones (Figure 3b, Text S1 in the Supporting Information S1). Mesoscale faults were commonly found in close proximity to map-scale faults and as such can be considered as part of their damage zones, but the distribution of mesoscale faults continued beyond the tip lines of some map-scale faults along strike into associated monocline limbs, indicating a genetic link between the faulting and monoclinal folding.

Due to shallow dip of the stratigraphic units in most of the study area, the axes of map-scale open folds were best defined from structure contours for marker horizons of the Boone Formation or the middle Bloyd sandstone of the Bloyd Formation (e.g., Figures 5 and 6) for which the elevation control points are included in published geologic

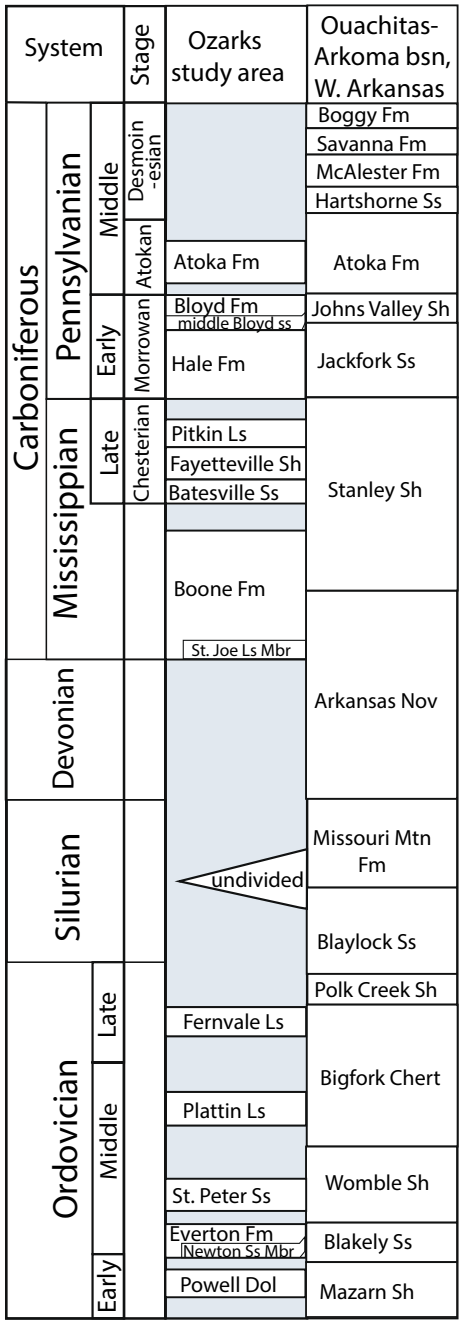

Figure 2. Stratigraphic correlations between Ozarks study area and Arkoma basin and Ouachita Mountains of western Arkansas (from McFarland, 1998). Bsn – basin, Dol – Dolomite, Fm – Formation, Mbr – Member, Nov – Novaculite, Ls – Limestone, Sh – Shale, Ss – Sandstone, ss – sandstone, W. – western.

maps. A large scatter of measured dip directions for bedding is inherent in shallowly dipping strata that underlie most of the study area (Figures 5 and 6), due to typical error sources in strike and dip measurements (e.g., Cruden & Charlesworth, 1976), but dip directions become consistent within moderately dipping fold limbs and help to define their extent. Most of the folds identified in this manner are monoclines with trends similar to, and commonly aligned with, map-scale faults. A few open anticlines and synclines are also recognized.

3.2. Fault Kinematic Measurements

Of 1,274 fault entries that were recorded at 452 sites (Figure 3b) in the study area (Hudson & Turner, 2022), 508 included measurement of fault orientation, slip direction, and slip sense (of varying degrees of confidence) needed for full kinematic analyses. Slip direction and sense were represented as total rake (Threet, 1973) of slip striae measured in the footwall clockwise relative to the fault strike, with broad categories of slip sense here used as normal (45°–134°), dextral (135°–224°), reverse (225°–314°), and sinistral (315°–360° and 1° to 44°). Slip senses were determined either from offset of preexisting features (e.g., bedding, older faults) or from asymmetric fault-surface features (Petit, 1987) such as Riedel fractures, calcite-growth fibers, or asymmetric polish of asperities.

3.3. Paleostress Analysis

Data from faults with full kinematic information were analyzed to calculate paleostress tensors in order to better refine the directions of principal stress axes with their associated error limits, as well as to help test for compatibility of subsets of the faults among different paleostress tensors. Using fault-slip data to estimate axes of paleostress or paleostrain tensors has become common practice, but a variety of techniques have been developed with different underlying assumptions (i.e., Angelier, 1984; Celerier et al., 2012; Hippolyte et al., 2012; Simon, 2018). To test for sensitivity of results to technique, each data set from the study area was analyzed in four types of inversions (Text S2 in the Supporting Information S1) based on the techniques of Angelier (1990), Michael (1984), and Sperner et al. (1993). In all cases, misfit angles of 45° or greater between actual slip direction and the maximum resolved shear stress on the same fault plane were used as a threshold to remove outliers, with groups of outlying faults subsequently inverted to test for different paleostress tensors. The 95% confidence regions about principal axes were estimated via a bootstrap resampling method. In general, the directions of principal stress axes yielded by the four techniques are similar within error limits, with principal differences between the methods being in the number of outliers excluded and in the resultant phi ratios $((\sigma_1-\sigma_2)/(\sigma_2-\sigma_3))$ for the tensors (Table S2). Based on these comparisons, a simple shear tensor summation (Sperner et al., 1993) was favored because it yielded smallest error regions around the principal stress axes and is appropriate for faults that are thought to be mostly newly formed. The simple shear tensor method follows Spang (1972) in assuming σ_2 axis lies in the fault plane perpendicular to the slip direction, whereas σ_1 and σ_3 axes are in the movement plane defined by the slip direction and the normal axis to the fault plane. The individual fault stress tensors are then averaged to give an estimate of the group stress tensor with deviation of the angle between σ_1 and the fault plane minimized among the faults in the set. A variant of the method was also applied in which the angle between the σ_1 axis and the slip vector was pre-set to 45°, in which case the tensor analysis becomes equivalent to the pressure-B axis-tension (P-B-T)

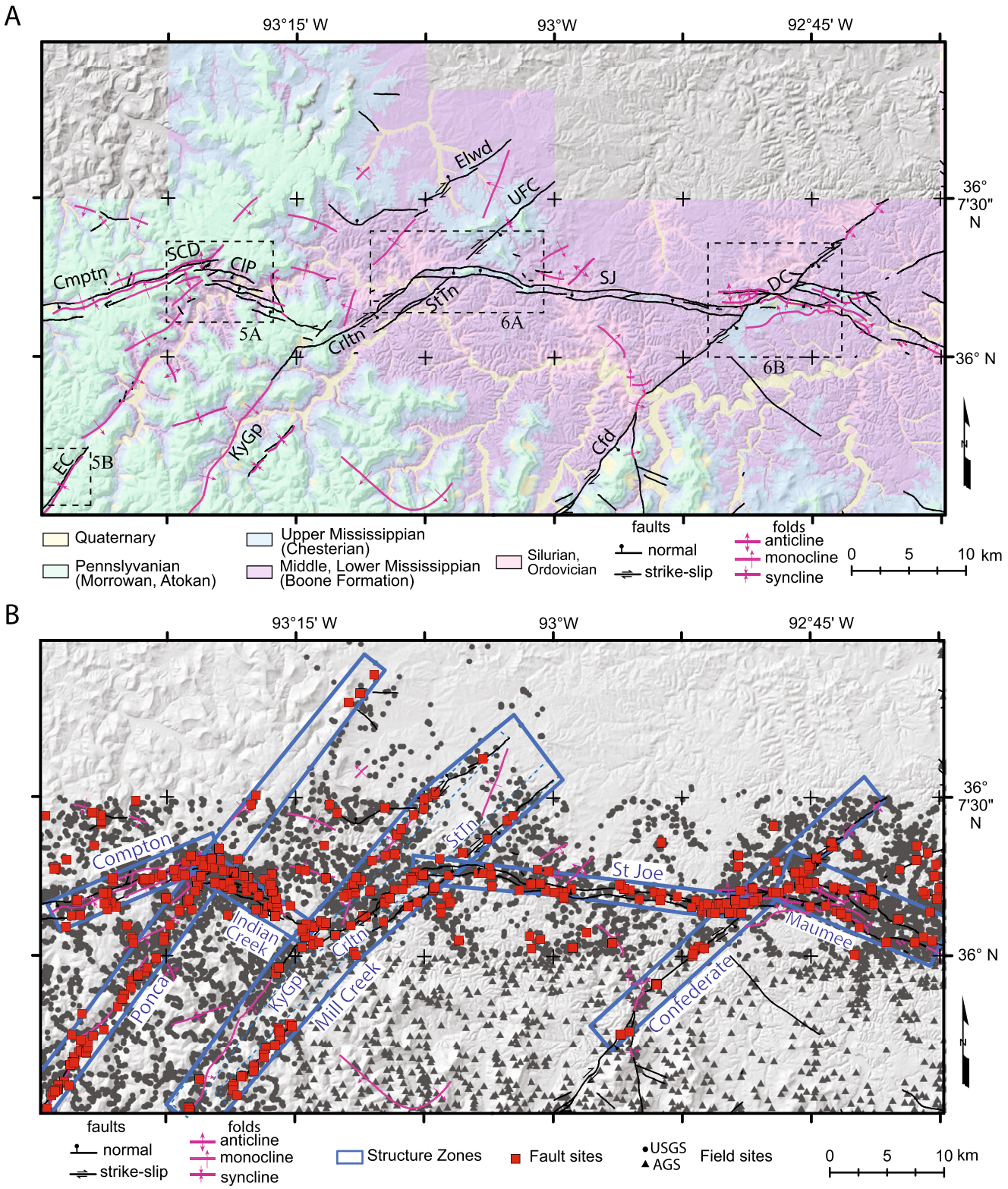

Figure 3. General geologic map of study area (a) with inset boxes (dashed lines) showing location of more detailed map diagrams of Figures 5 and 6. Fault, fold, and structural subzone names are Confederate, Cfd; Compton, Cmptn; California Point, ClP; Carlton, Crltn; Davy Crockett, DC; Edgemon Creek, EC; Elmwood, Elwd; Keys Gap, KyGp; Sneeds Creek dome, SCD; Stringtown, StTn; St. Joe, SJ; and Upper Flatrock Creek, UFC. (b) Locations of all fault sites versus field sites. Structural zones discussed in text are shown as labeled blue boxes. USGS – U.S. Geological Survey, AGS – Arkansas Geological Survey.

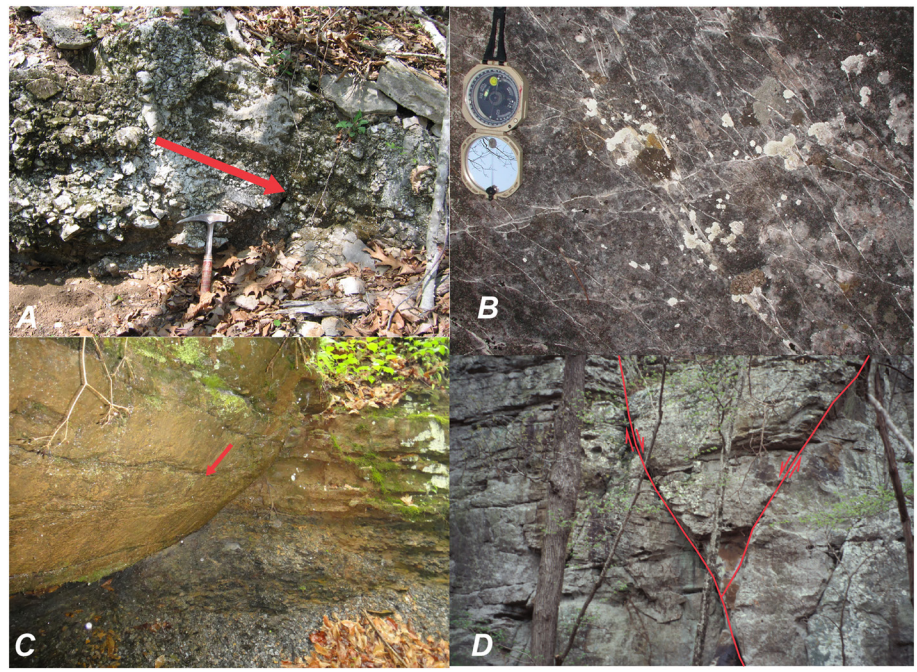

Figure 4. Examples of representative fault styles developed in different lithology types within the study area. Photographs include (a) chert breccia with shallowly plunging mullions (red arrow) in limestone of Mississippian Boone Formation, (b) conjugate strike-slip deformation bands cutting Ordovician sandstone, (c) fine-wear striae (red arrow) on normal fault cutting Pennsylvanian sandstone, (d) conjugate normal faults forming small graben in Pennsylvanian sandstone.

scale-invariant, infinitesimal strain model of Marrett and Allmendinger (1990). The agreement among principal axes whose methods infer paleostress versus infinitesimal strain suggest that in the foreland geologic setting of the study area, σ_3 paralleled infinitesimal extension and σ_1 paralleled infinitesimal shortening (Text S3 in the Supporting Information S1).

At outcrop scale, it was common to observe two dominant sets of faults with opposing slip senses that in some sites are mutually offsetting (Figure 4). These fault sets have geometries as described for newly formed conjugate fault sets of Anderson (1951) and were observed for normal, strike-slip, and reverse slip fault types. If slip striae were not preserved on the faults (e.g., as common for deformation bands) and if a sufficient number of planes could be measured to define dual orientation clusters, qualitative estimates of σ_1 and σ_3 paleostress axes at the sites were made by bisecting the acute and obtuse angles, respectively, between the fault sets (Text S3 in the Supporting Information S1, Table S3), to augment the more robust paloestress inversions determined from kinematic data.

4. Results

4.1. Map-Scale Fault and Fold Characteristics

4.1.1. Structural Zones

The restricted spatial distribution of both map-scale and mesoscopic faulting indicates that deformation was concentrated in several linear structural zones whose orientations span a range from northeast to west-northwest (Figure 3b). These zones envelope arrays of discontinuous, often en echelon normal and strike-slip faults and linking monoclinal folds. Salient characteristics of seven structural zones are discussed next, beginning in the west and moving east. An assessment of whether the structural zones may have formed by reactivation of underlying basement weaknesses is discussed later.

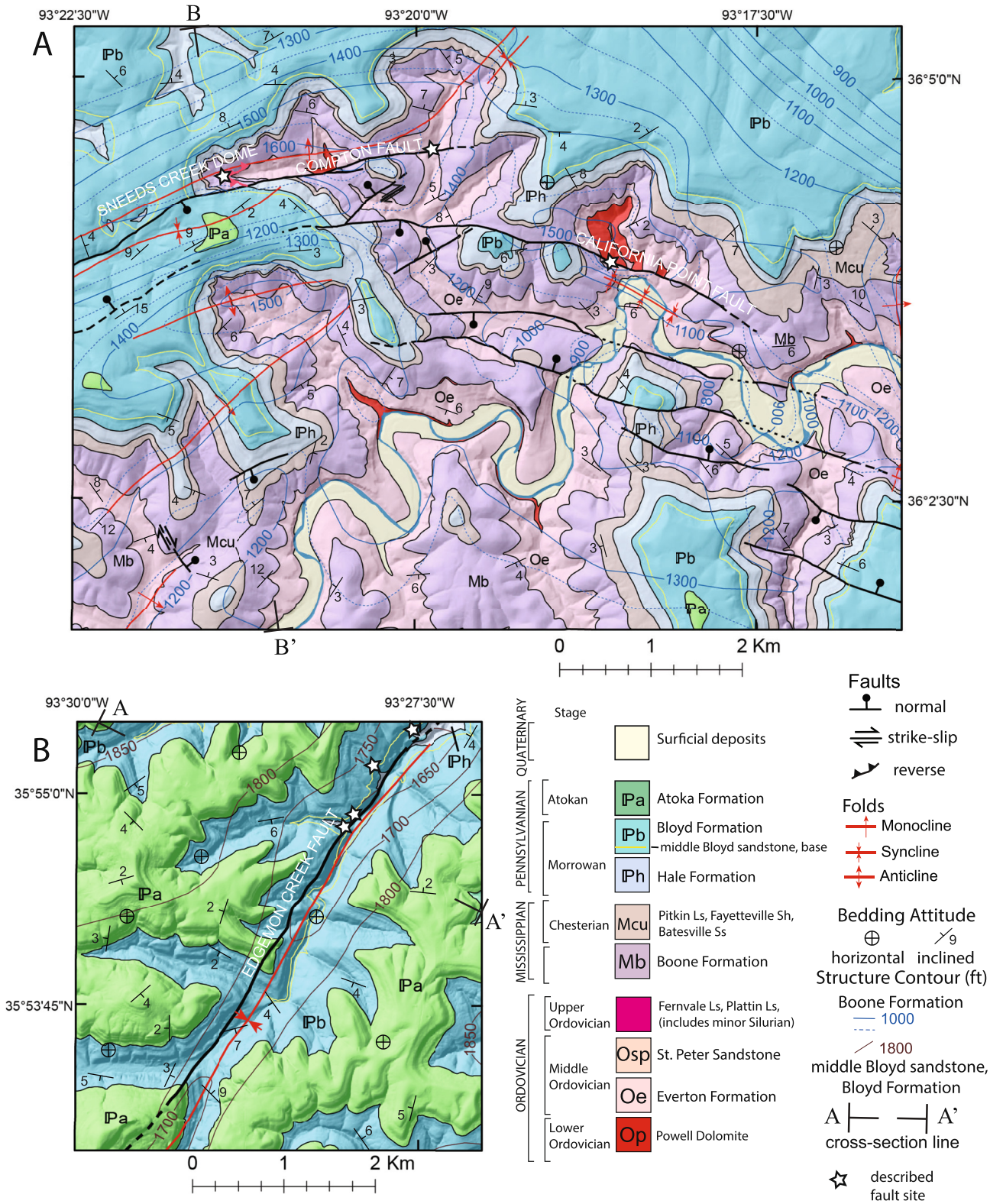

Figure 5. Detailed geologic maps for selected areas shown in Figure 3A. White stars show fault sites discussed in text. Cross-section profiles shown in Figure 7.

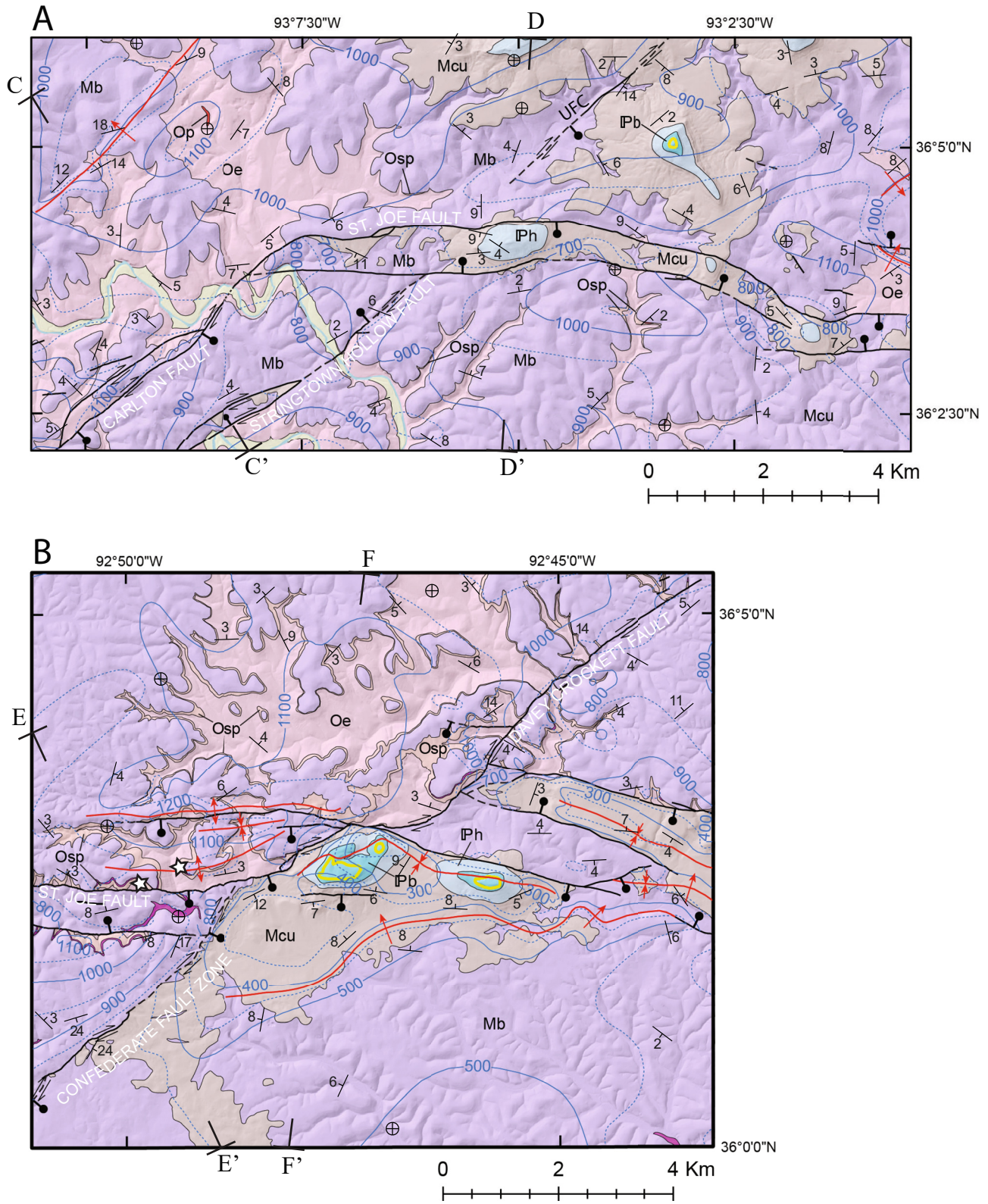

Figure 6. Detailed geologic maps for selected areas shown in Figure 3. White stars show fault sites discussed in text. Legend as in Figure 5. Cross-section profiles shown in Figure 7.

4.1.1.1. Compton Zone

The N65°E Compton structural zone (Figure 3) is mostly focused on the down-to-the-southeast Compton fault (Figure 7b) with a paired alignment of down-to-the-northwest faults and monoclinal folds on its southern side. These structures give the zone an overall graben form. The Compton fault has up to 120 m of throw that decreases gradually to the southwest (Turner & Hudson, 2018), but abruptly to the northeast (Hudson & Turner, 2014a) where it intersects the Ponca zone. Some exposures of Upper Mississippian and Pennsylvanian sandstones interbedded with shale intervals dip steeply immediately adjacent to the Compton fault.

4.1.1.2. Ponca Zone

The Ponca zone is a long, narrow, N35°E trending zone of faults and monoclinal folds with consistent down-to-the-southeast throw that varies from 45 to 90 m along strike (Hudson & Turner, 2007, 2014a; Turner & Hudson, 2018). A shallow trough is commonly preserved at the immediate base of the overall monoclinal limb and is in the immediate hanging wall of the Egdemon Creek fault (Figures 5b and 7a). The limbs of several monoclinal folds have strikes that are rotated clockwise from the overall trend of the Ponca zone and both faults and folds have left-stepping, en echelon patterns. The zone coincides with alignments of lead-zinc mineral deposits (McKnight, 1935) and topographic features that define the Ponca lineament of McFarland (1988).

4.1.1.3. Indian Creek Zone

The N60°W trending Indian Creek zone encompasses seven nested normal faults, such as the California Point fault, arranged in a right-stepping, en echelon pattern (Figure 5a) (Hudson & Turner, 2014a). Strata are dropped over 210 m in the center of the zone relative to the flanks, giving the zone the form of a nested graben. The individual faults have maximum throw mostly less than 40 m.

4.1.1.4. Mill Creek Zone

The Mill Creek zone is a 5-km-wide zone that trends N40°E overall. In detail it can be broken into three subzones; two parallel thinner subzones and a bridging subzone. The Keys Gap-Elmwood subzone trends N38°E along the northwestern edge of the Mill Creek zone and is defined from both structure contours and an alignment of fault sites. The down-to-the-northwest throw of the Elmwood left-stepping, en echelon fault zone at the northeast end (Hudson & Turner, 2014a) is opposite of the down-to-the-southeast folding across the Keys Gap monocline in the southwest (Figure 3a) (Hudson & Turner, 2016). The N44°E rending Stringtown subzone has variable throw and defines the southeastern side of the Mill Creek zone. On the northeast end, the Upper Flatrock Creek fault aligns along strike with the Stringtown fault zone (Figure 6a) but without apparent offset of the intervening St. Joe graben (Hudson & Turner, 2014a). The southwest end of the Stringtown subzone includes two left-stepping en echelon, down-to-the-southeast faults and related hanging wall synclines (Hudson & Turner, 2016); additional deformation along strike to the northeast of these faults is likely covered by Quaternary alluvium along the Little Buffalo River (Chandler & Ausbrooks, 2003). The N59°E trending Carlton subzone is centered on the Carlton fault and bridges the gap between its junctions with the St. Joe fault and Stringtown subzone on the northeast and the intersection with the Keys Gap zone on the southwest. The Carlton fault has overall down-to-the-southeast throw, but includes an adjacent central block bounded by a fault with opposed throw (Figures 6a and 7c).

4.1.1.5. St. Joe Zone

The N84°W trending St. Joe zone (Figure 3) is focused on the south-dipping St. Joe normal fault on its northern edge (Hudson & Turner, 2014a). At over 30 km in length, the St. Joe fault is the longest continuous fault in the study area and has as much as 150 m of down-to-the-south throw. Although continuous, the St. Joe fault has segments of abrupt curvature (Figures 3 and 6a) that indicate it probably coalesced from separate segments during fault growth. Three shorter, right-stepping, north-dipping normal faults oppose the St. Joe fault to the south (Figure 3) to collectively form a graben complex (Figure 7d).

4.1.1.6. Confederate Zone

This N47°E trending zone has dextral, down-to-the-southeast oblique throw (Figures 7e and 7f). More northerly trending monoclines form linking relay ramps between left-stepping en echelon faults (Figure 3) in the southwestern and northeastern parts of the zone (Chandler & Ausbrooks, 2015a; Hudson & Turner, 2014a), whereas the zone takes a right step at its intersection with the St. Joe and Maumee zones (Figures 3a and 6b).

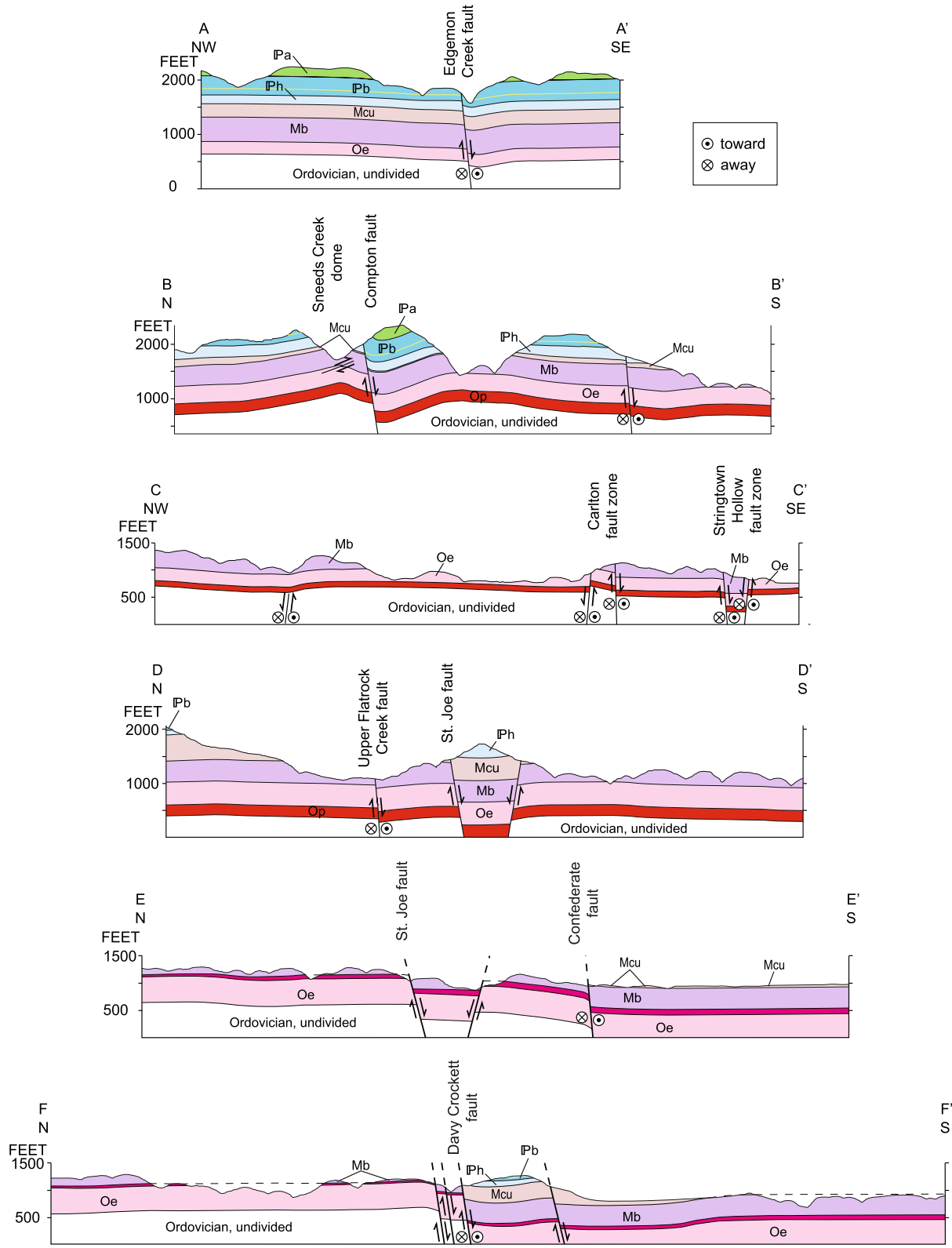

Figure 7. Cross sections for profiles, arranged from west to east, for geologic maps shown on Figures 5 and 6. Map units are symbolized same as in Figure 5, except that Middle Ordovician St. Peter Sandstone is combined with Upper Ordovician units. All cross sections have 2X vertical exaggeration and are modified from published geologic map cross sections of (a) Hudson & Turner, 2007, (b) Hudson & Murray, 2003, (c) Hudson et al., 2001, (d) Hudson & Murray, 2004, and (e and f) Hudson & Turner, 2009.

4.1.1.7. Maumee Zone

The N65°W-trending Maumee zone is broad and with more diffuse fault sites than the other structural zones. It includes a set of mostly west-northwest striking normal faults that merge with or terminate against (Figure 6b) the northeast-trending Confederate structural zone (Hudson & Turner, 2009; Turner & Hudson, 2010).

4.1.2. Strain Transfer of Extension

Although deformation in the study area is separated into several linear structural zones, faults within these zones intersect and change throws in a manner that indicate there was strain transfer (e.g., Faulds & Varga, 1998; Peacock, 2002) among the different structural zones (Hudson et al., 2006). Zones with more easterly strikes (Compton, Indian Creek, St. Joe, and Maumee) are predominantly extensional (Figures 7b and 7d) but are spatially offset from each other across the intervening northeast-trending Ponca, Mill Creek and Confederate structural zones, for which overall normal-right-lateral oblique offset is interpreted (Figures 7a–7e, 7f) based on the slip-sense of faults within these zones. Examples of strain transfer via hard linking (Peacock et al., 2000) include the eastern end of the St. Joe normal fault that curves and overlaps the Davy Crockett fault of the northeast-trending Confederate structural zone (Figure 6b). Similarly, the western end of the St. Joe fault loses throw west of the intersection with the Stringtown subzone and then farther west merges with the northeast end of the Carlton fault (Figure 6a). Although not hard linked to an individual fault, the southwestern end of the Carlton fault overlaps with the southeastern end of the Indian Creek zone (Figure 3). The northwest end of the Indian Creek zone overlaps the intersection of the Ponca and Compton structural zones (Figure 5a) and northeast of this intersection the Ponca structural zone loses throw (Figure 3). Strain transfer among the different structural zones indicated by these spatial relations indicates there was broadly contemporaneous extensional deformation among the different structural zones.

4.2. Fault-Slip Analyses

4.2.1. Statistics

Summary statistics (Figure 8a) for faults with full kinematic data show that most dip steeply (60° or greater). In contrast to the bimodal northeast and west-northwest strikes of map-scale faults (Figure 3), the strike frequency of the total fault population is dominated by east-west striking faults, due to a predominance of mesoscale normal faults that are mostly responsible for the strong total-rake frequency peak at 90°. There is also a significant population of faults with oblique dextral normal slip (total rakes from 110°–160°). Moderate total-rake frequency peaks centered at 0° and 180° demonstrate the common presence of sinistral and dextral strike-slip faults, respectively, whereas a small but discrete total-rake peak at 270° marks subordinate reverse faulting. Among faults with oblique slip, those having dextral-normal sense are most common. The faults from which kinematic data were collected are subequally distributed within the Ordovician, Mississippian and Pennsylvanian rock units, although, a large proportion of data from Pennsylvanian units were concentrated in the middle Bloyd sandstone of the Bloyd Formation. Separated by age of host rock, faults in both Ordovician and Mississippian strata show similar mixtures of normal and strike-slip faulting whereas Pennsylvanian strata have a stronger predominance of normal faults (Figures 8b and 8c).

4.2.2. Fault Deformation Phases

Three phases of late Paleozoic deformation have been previously identified in the study area (Hudson & Cox, 2003; Hudson & Murray, 2003), with age constraints derived from the age of the strata they affect and from offsetting relationships among the different faults. The oldest is a spatial-limited phase (D1) of reverse faulting and folding that accommodated east-northeast directed shortening that was active during and caused large unit thickness variations of strata in the latest Mississippian to earliest Pennsylvanian (Hudson & Murray, 2003; Hudson & Turner, 2014b). The D1 phase cannot be simply linked to growth of the Ouachita orogen to the south and thus the details of its deformation characteristics and timing constraints will be described elsewhere. The last two phases are the widespread north-south extension (D2) accommodated by most map-scale structures and a subsequent phase of north-south shortening (D3). The D2 and D3 phases of this study compare to the first and second phases of regional deformation in the Ozark plateaus region of Cox (2009).

The succession from D2 to D3 fault phases is documented from cross-cutting field relations at several sites. At a site near the intersection of the Compton and Ponca structural zones (Figure 5a), a typically porous,

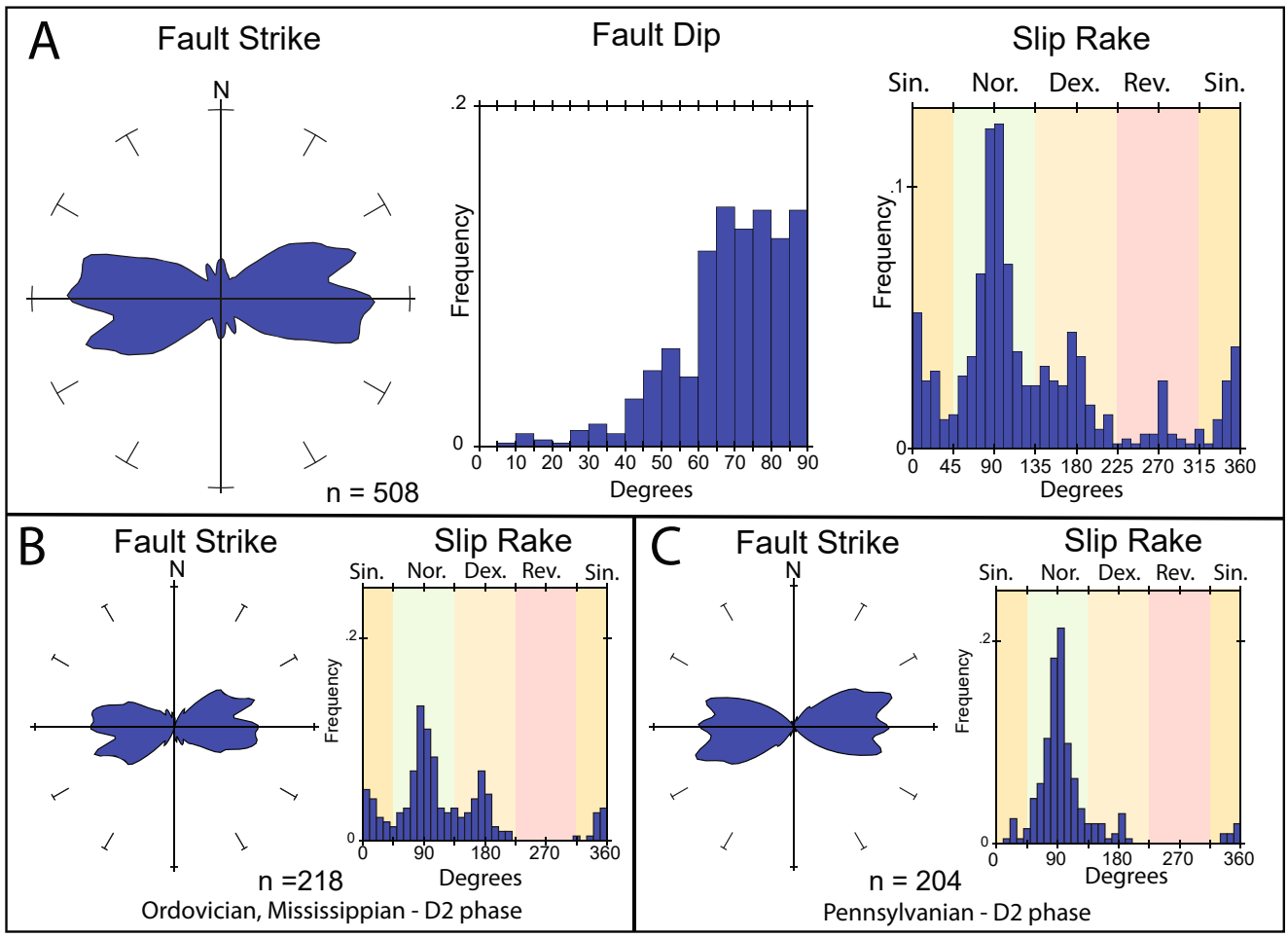

Figure 8. Summary statistics of strike, dip, and total rake distributions for faults with kinematic data in the study area. Rose diagram of fault strike shows smoothed values over 10° bins. Sin., sinistral; Nor., normal; Dex., dextral; Rev., reverse. (a) All data. (b) Data from Ordovician and Mississippian strata compatible with D2 deformation phase. (c) Data from Pennsylvanian strata compatible with D2 deformation phase.

carbonate-cemented Newton Sandstone Member of the Ordovician Everton Formation in the hanging wall of the Compton fault contains conjugate sets of normal-sense deformation bands that record D2 extension (Figure 9b) and both the sandstone host rock and deformation bands are silicified. A later conjugate set of strike-slip faults that have fine wear striae and small Riedel flakes (Figure 9a) that indicate slip sense cut the silicified sandstone and record D3 north-south shortening (Figure 9c). Here, the D2 to D3 succession is indicated by both cross-cutting relations and the change in faulting style from deformation bands in porous sandstone to fine wear striae after porosity loss due to silicification. At another site (Figure 5b) in the southwest end of the Ponca structural zone (Hudson & Turner, 2007), middle Bloyd sandstone of the Pennsylvanian Bloyd Formation near the Edgemon Creek fault has deformation bands and striated normal and strike-slip faults that record north-south extension (Figures 9d and 9e), which are offset by north-trending silicified strike-slip faults indicative of north-south shortening (Figures 9d and 9f).

4.2.3. Paleostress Analyses

Separating the fault data based on their compatibility with paleostress tensors yielded four sets of faults of decreasing number (Figure 10) that are considered as two broad groups corresponding to the D2 and D3 deformation episodes: (a) normal faults or strike-slip faults in which the σ_3 axis was north-south directed and subhorizontal, and (b) strike-slip faults or a less common set of reverse faults in which the σ_1 axis was north-south directed and subhorizontal. The normal- and reverse-fault groups could be separated beforehand by sorting on total rake values to achieve good data compatibility within their respective paleostress tensors. In contrast, separating the strike-slip faults based on association with the D2 and D3 phases required separation of misfit outliers

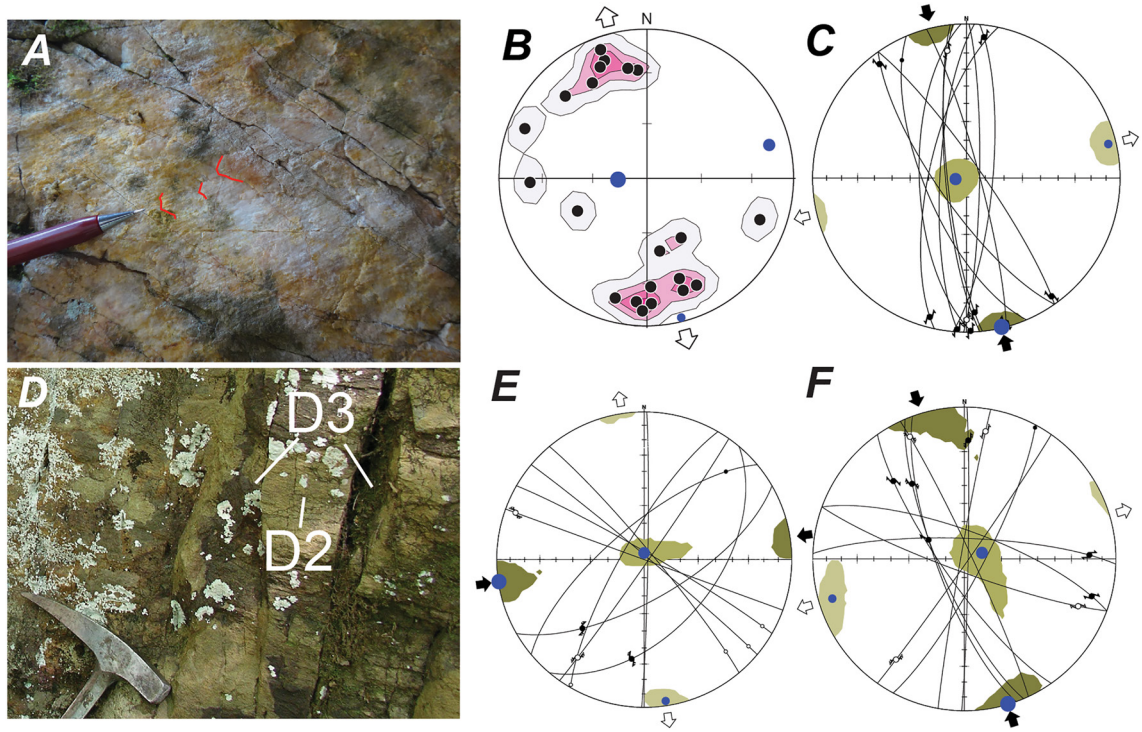

Figure 9. Examples of field sites with cross-cutting relations between D2 and D3 fault phases. For all fault-slip analyses, large, medium, and small blue circles represent maximum, intermediate, and minimum principal-stress axes, respectively, with surrounding colored regions indicating 2 sigma error limits estimated from bootstrap technique. Outer white and black arrows show directions of horizontal extension and compression, respectively. Arcs and dots are lower hemisphere projections of fault planes and their slip lines, respectively. Small arrows show movement sense of hanging wall block. (a) For site in Compton fault hanging wall, fault plane in silicified sandstone with fine wear striae and Reidel flakes (accented with red lines); (b) frequency contour of D2 deformation bands in hanging-wall of Compton fault and causative principal stress axes (arrows and blue dots) inferred from conjugate normal fault geometry; (c) fault-slip analysis for overprinting strike-slip faults. (d) For site in Pennsylvanian sandstone in southwest part of study area, photo of D2 fault plane offset by D3 fault planes. (e) Fault-slip analysis for older D2 strike-slip faults cut by (f) D3 strike-slip faults.

and the inversion of the resulting subsets. These actions of presorting by total-rake value and further separation of misfit outliers were successful in replicating the different phases of fault timing observed from cross-cutting relationships at field sites. A small group of faults preserved multiple sets of striations on their planes, some with evidence of relative timing. Inversion of this data set included the older striae with normal and strike-slip senses to yield a stress tensor compatible with D2 extension (Figure 10e).

4.2.3.1. D2 North-South Extension

Consistent with the geologic map constraints indicating that most of the map-scale structures identified within the study area accommodated extension or trans tension (Figure 7), normal faults and strike-slip faults of the D2 group are most numerous and are widely distributed. Normal faults have both strong north-dipping and south-dipping modes (Figure 10a), although with significant spatial variations of strike. Likewise, the D2 strike-slip faults comprise predominantly northeast-striking dextral faults or slightly less common west-northwest-striking sinistral faults.

The overall paleostress tensors recording D2 extension show good coherence, but analyzing the fault data separately from the different structural zones highlights spatial variability in both the relative proportions of normal and strike-slip faults as well as the azimuths of the σ_3 axes (Figure 11). Faults from the west-northwest trending Indian Creek, St. Joe and Maumee structural zones have a predominance of normal faulting and azimuths of σ_3 with south to south-southwest trends. The northeast-trending Ponca, Mill Creek, and Confederate structural zones include significant populations of dextral and sinistral strike-slip faults in addition to normal faults and estimated azimuths of their σ_3 axes range from south-southeast to south-southwest. Faults from the east-northeast trending Compton structural zone are predominantly normal sense but with a highest rake frequency skewed toward dextral normal oblique motion.

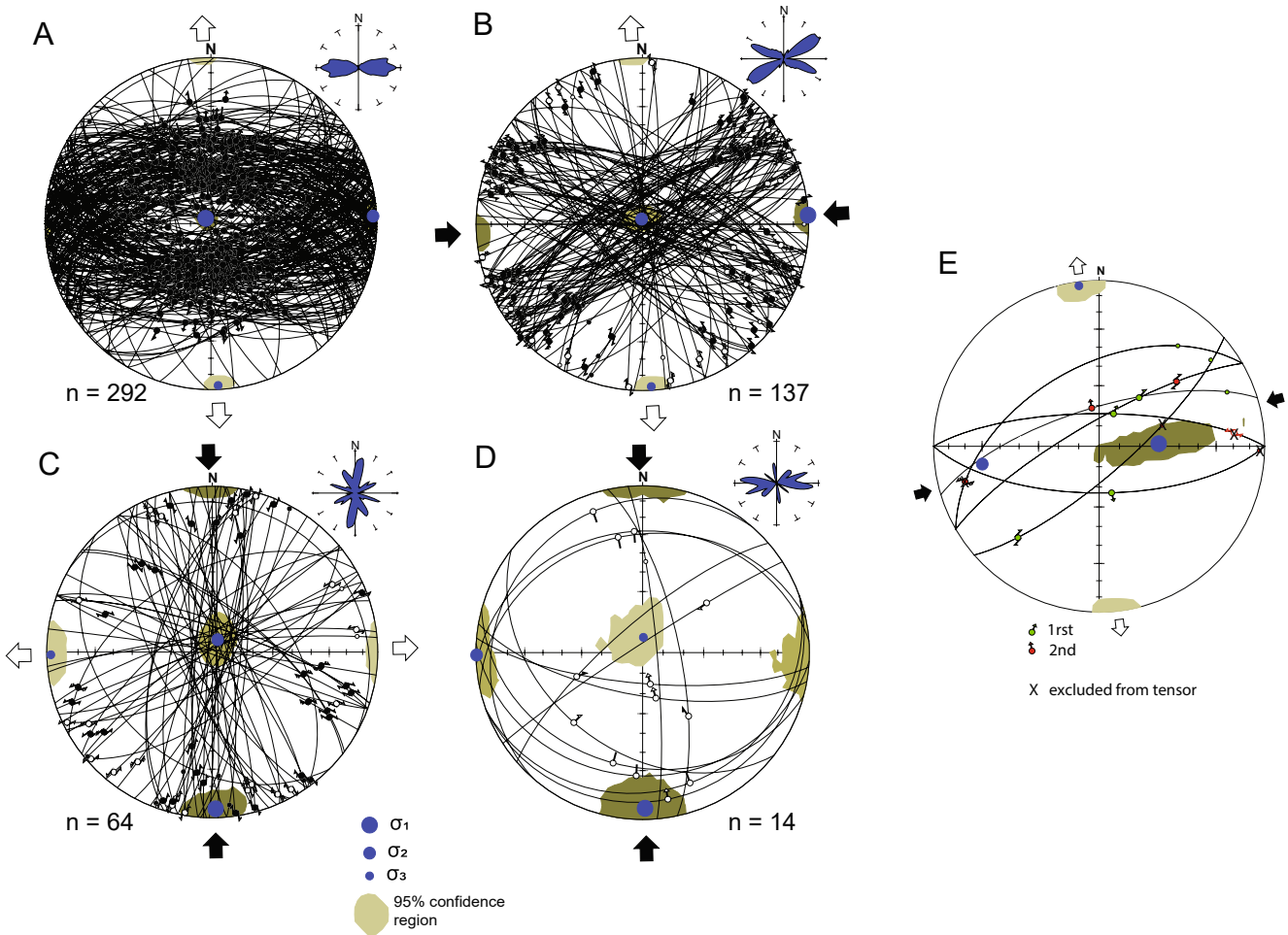

Figure 10. Summary fault tensor equal-area nets and associated fault-strike rose diagrams (to upper right of equal-area nets) for D2 groups of (a) normal, and (b) strike-slip faults, and D3 groups of (c) strike-slip faults and (d) reverse faults. (e) For fault planes with multiple striations, fault tensor solution includes older striae that accommodate north-south D2 extension. For each equal-area net, arcs represent fault planes and arrows represent slip directions. Large, medium, and small blue circles represent maximum, intermediate, and minimum principal-stress axes, respectively, with surrounding colored regions indicating 2 sigma error limits estimated from bootstrap technique. Outer white and black arrows show directions of horizontal extension and compression, respectively.

4.2.3.2. D3 North-South Shortening

Faults that accommodated north-south shortening during the subsequent D3 phase are predominantly of strike-slip sense (Figure 10c). Spatially, most of these strike-slip faults are concentrated within the northeast-trending structural zones (Figure 12), although a few are found at the edges of the more westerly striking structural zones such as in the immediate footwall of the St. Joe normal fault (Figure S6-1b in the Supporting Information S1). Sets of north-northwest-striking dextral and north-northeast-striking sinistral faults are the most common and include newly formed faults cutting silicified sandstone at several sites (e.g., Figure 9c). Lesser subsets of west-northwest- or northeast-striking D3 strike-slip faults likely reactivated earlier D2 fault planes that have similar strikes (Figure 9b).

Dip-slip reverse faults resulting from north-south shortening are few (Figure 12). In the western part of the study area, a low-angle fault with south-southwest-trending striae (Figure 13) interpreted as thrust offset of the basal St. Joe Member of the Boone Formation (Figures 5a and Figure 7b) was found near the crest of the east-northeast-elongate Sneed Creek dome (Croneis, 1930; Hudson & Murray, 2003). At a second locality on a well-exposed plane of the California Point fault, asymmetric silica growth fibers (Figure 13) observed in a localized area record an episode of reverse sense slip, although the overall displacement on the fault is of normal sense.

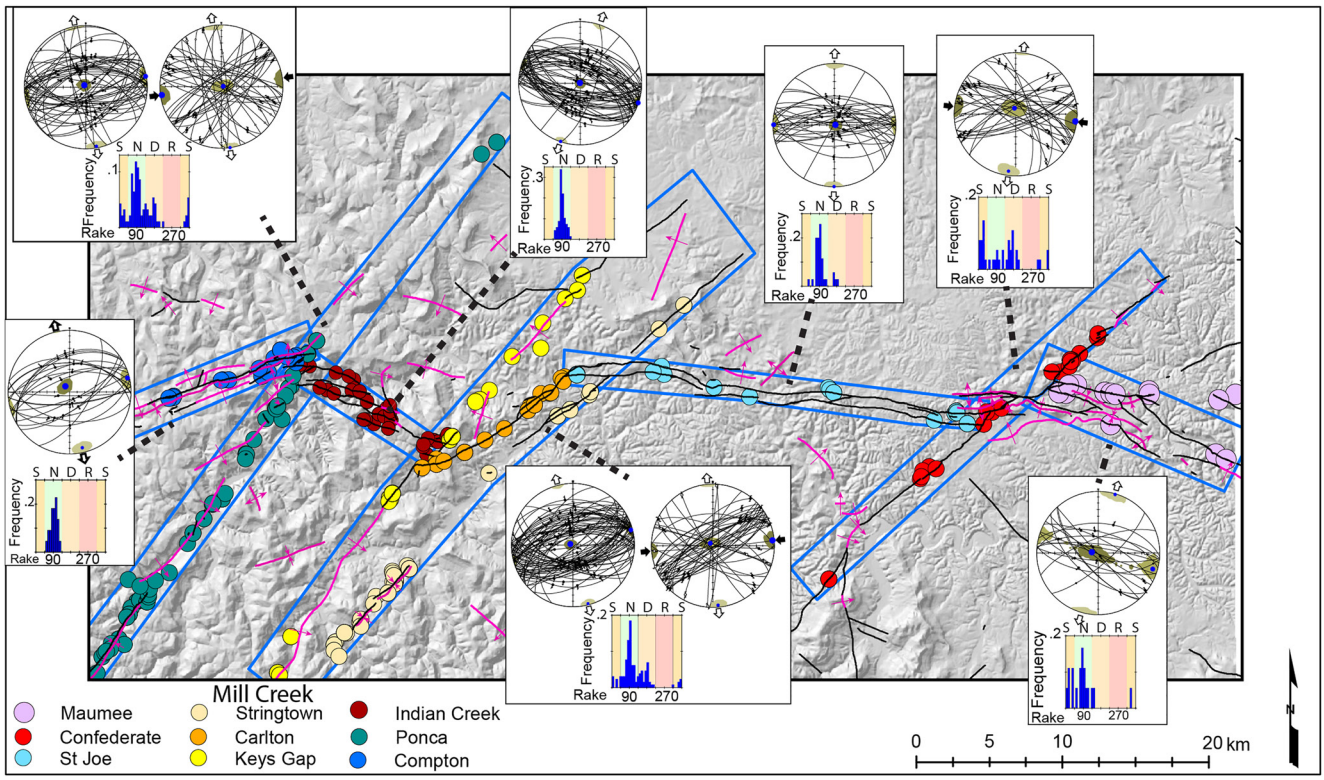

Figure 11. Spatial variability of faulting associated with D2 extension among different structural zones. Colored dots on map indicate sites associated within different structural zones used to invert for normal or strike-slip faulting stress tensors. Rake histograms (N, normal; D, dextral; R, reverse, S, sinistral) illustrate varying proportions of normal and strike-slip faults that accommodated D2 extension within each structural zone. Map symbols as in Figure 3 and symbology for equal area nets described in Figure 9.

A second eastern area with low-angle thrust faults was found at sites about 100 and 400 m internal to the footwall of the St. Joe normal fault near its intersection with the Confederate structural zone (Figure 6b). Both sites in Ordovician St. Peter Sandstone contain oppositely dipping sets of low-angle deformation bands, some with reverse offset (Figure 13d). The σ_1 axis of their interpreted conjugate pairs and slip striae on a few planes indicate north-south shortening (Figure 13e). Folding is locally developed in a paired set of east-west-trending open synclines and anticlines coincident and just to the north of the fault sites (Figure 6b).

5. Discussion

The evolution from north-south extension to north-south shortening in response to the developing Ouachita orogeny is recorded in the geometry and succession of foreland structures in the southern flank of the Ozark dome. The configuration of mesoscopic faults and folds as well as the paleostress tensors determined from fault kinematic data from the study area are discussed in light of (a) the likely role of preexisting weaknesses in localizing extensional deformation and their comparison to oblique rift models, (b) the tectonic setting of extension in the foreland basin system, (c) the change to north-south shortening and evidence for incipient inversion, and (d) the spatial and temporal relations between faulting and late Paleozoic regional fluid flow.

5.1. Flexural Extension

Although several phases of deformation have been detected on the southern flank of the Ozark dome (Chinn & Konig, 1973; Cox, 2009; Hudson, 2000; Hudson & Cox, 2003), the systematic inspection during geologic mapping for this study demonstrates that structures that accommodated north-south extension are the most widespread and have the largest offsets across the Buffalo River watershed area (Figure 3). Most faults within the study area retain normal or normal-oblique cumulative offsets (Figure 7), despite the evidence for slip reversal on some

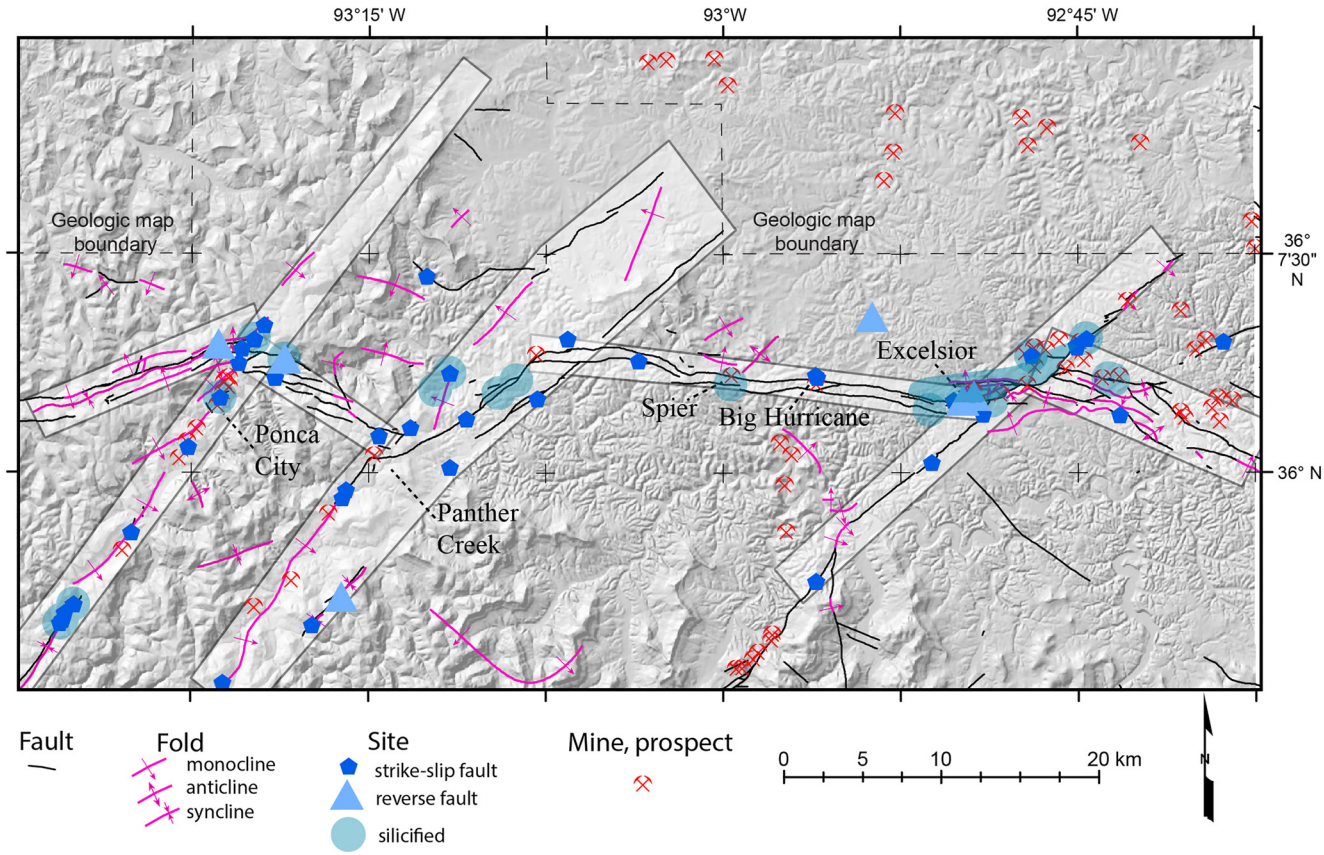

Figure 12. Spatial distribution of fault sites associated with D3 shortening. Also shown are fault sites with silicification. Locations and names of lead-zinc mines and prospects from McKnight (1935).

faults. Monoclinal folds are best explained as forced folds over buried faults (Hardy & McClay, 1999; Withjack et al., 1990) having normal or normal-oblique offsets, as indicated by the colinear alignments of faults and monoclines within the different structural zones. Within the northeast-trending structural zones, the left-stepping en echelon arrangement of faults and monoclinal folds along with the common presence of localized troughs at their base (Figures 5b, 7a, and 7b) are similar to elements of negative flower structures (Harding, 1985) that develop in transtension. Among the population of faults with kinematic data, about 70% can be fit to either normal or strike-slip paleostress tensors with shallowly inclined σ_3 axes having approximately north-south azimuths.

5.1.1. Preexisting Basement Weaknesses Reactivated in Oblique Extension

Several lines of evidence suggest that flexural extension within the Arkoma foreland basin system and more specifically within the study area was controlled at least in part by reactivation of preexisting basement weaknesses. For example, the relatively narrow breadth of the foredeep Arkoma basin is consistent with a reduced wavelength of broken-plate models of lithospheric flexure whose elastic strength is lessened due to preexisting crustal weaknesses (DeCelles, 2012; Thomas, 2004; Waschbusch & Royden, 1992). Furthermore, northeast- and west-northwest-trending structural zones in the study are parallel to commonly recognized basement fault zones throughout the midcontinent region (Marshak & Paulsen, 1996; Thomas, 2006) and within the Ozark plateaus region (Cox, 2009; Starbuck, 2017) and for which Phanerozoic reactivations have been documented (Marshak et al., 2000). Structure-zone trends are also similar to the common northeast and northwest trends prevalent in regional geophysical anomaly maps (Hildenbrand et al., 1996; McCafferty et al., 2019) whose expressions are thought to follow lithologic boundaries and fault zones in Mesoproterozoic crystalline basement (Van Schmus et al., 1996; Whitmeyer & Karlstrom, 2007). Within the study area, recently acquired high-resolution aeromagnetic data (McCafferty & Brown, 2020) demonstrate alignments or truncations of magnetic anomalies that coincide with the independently defined surface structural zones, supporting the interpretation that their locations were controlled by basement elements (Text S4 in the Supporting Information S1).

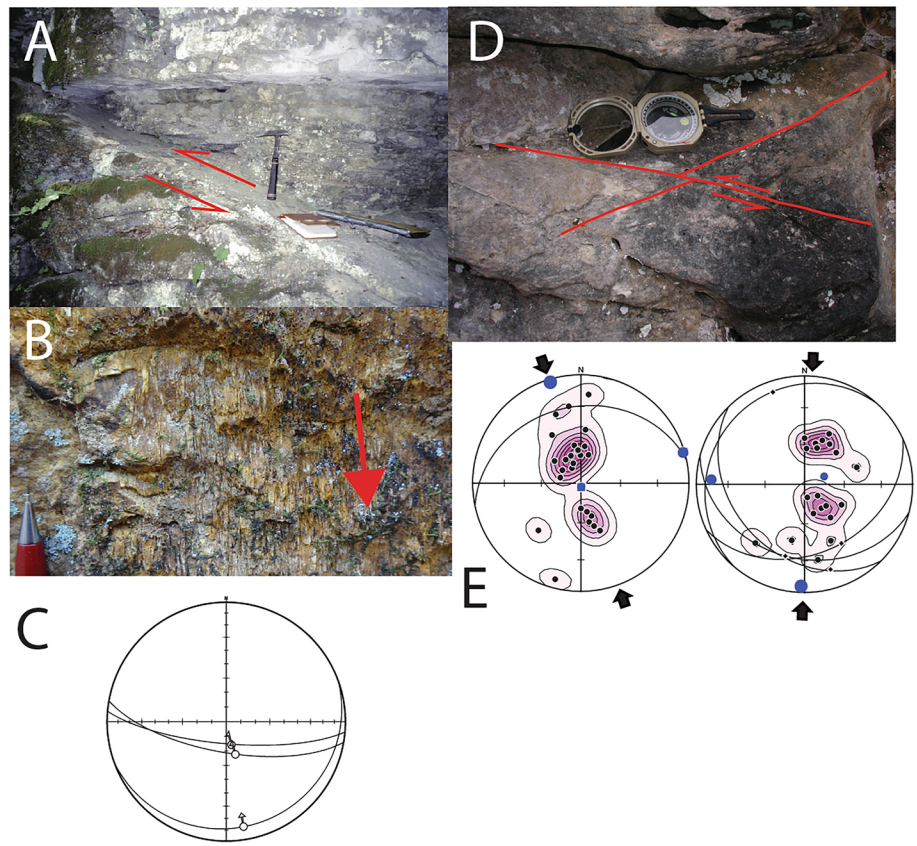

Figure 13. Examples of reverse faults associated with D3 shortening. (a) Low-angle fault cutting St. Joe Limestone Member of Boone Formation in footwall of Compton fault. (b) Hanging wall of overhanging California Point normal fault plane with fibrous quartz deposits that record episode of reverse slip. (c) Equal area net of planes and slip striae for reverse faults of A and B. (d) Low angle deformation bands in Ordovician St. Peter Sandstone near St. Joe, AR that record reverse offset. (e) Equal area nets of two sites with frequency contour of deformation bands and principal stress axes inferred from conjugate geometry. Large, medium, and small blue circles represent maximum, intermediate, and minimum principal-stress axes, respectively, and outer black arrows show directions of horizontal compression.

Independent evidence for the influence of basement weaknesses in the study area comes from the match of the D2 extensional deformation in structural zones to characteristics predicted for oblique rifts (Figure 14). Experimental and analytical studies of oblique rifting document structures developed in cover strata over elongated weak zones (Tron & Brun, 1991; Withjack & Jamison, 1986) or buried faults (Schlische et al., 2002). These models predict changes in fault patterns and horizontal extension directions that are dependent on the angle of obliquity, α, between the trend of the structural zone and the direction of divergence of adjacent blocks across the zone (Clifton et al., 2000; Withjack & Jamison, 1986), or its complementary angle, the rift obliquity (Figure 14a). For α of 90°, divergence is normal to the zone and normal faults form with strikes parallel to the rift trend. At moderate obliquity (α values 75°–45°) the zone undergoes transtension accommodated by en echelon sets of normal faults whose strikes are rotated at about half of the α angle from zone trend. For lower values of α between 45° and 30°, transtension is accommodated by sets of both normal and strike-slip faults whereas for α less than about 22.5° the models predict that strike-slip faults dominate.

Characteristics of D2 structures in the study area consistent with oblique rift models are (a) the common en echelon arrangement of faults of both left- and right-stepping arrays and (b) an orientation dependency for structural zones of both the relative abundances of normal and strike-slip faults and the paleostress directions. The divergence of extensional directions found among differently oriented structural zones is used for a test of the predicted stress refraction within the deforming zones. A significant correlation ($R^2 = 0.69$) found between in situ σ_3 azimuths and the trends of the different structural zones is consistent with stress refraction in weak zones (Figure 14b). For example, the 199° ± 6° azimuth of the σ_3 axis from the west-northwest-trending Indian Creek

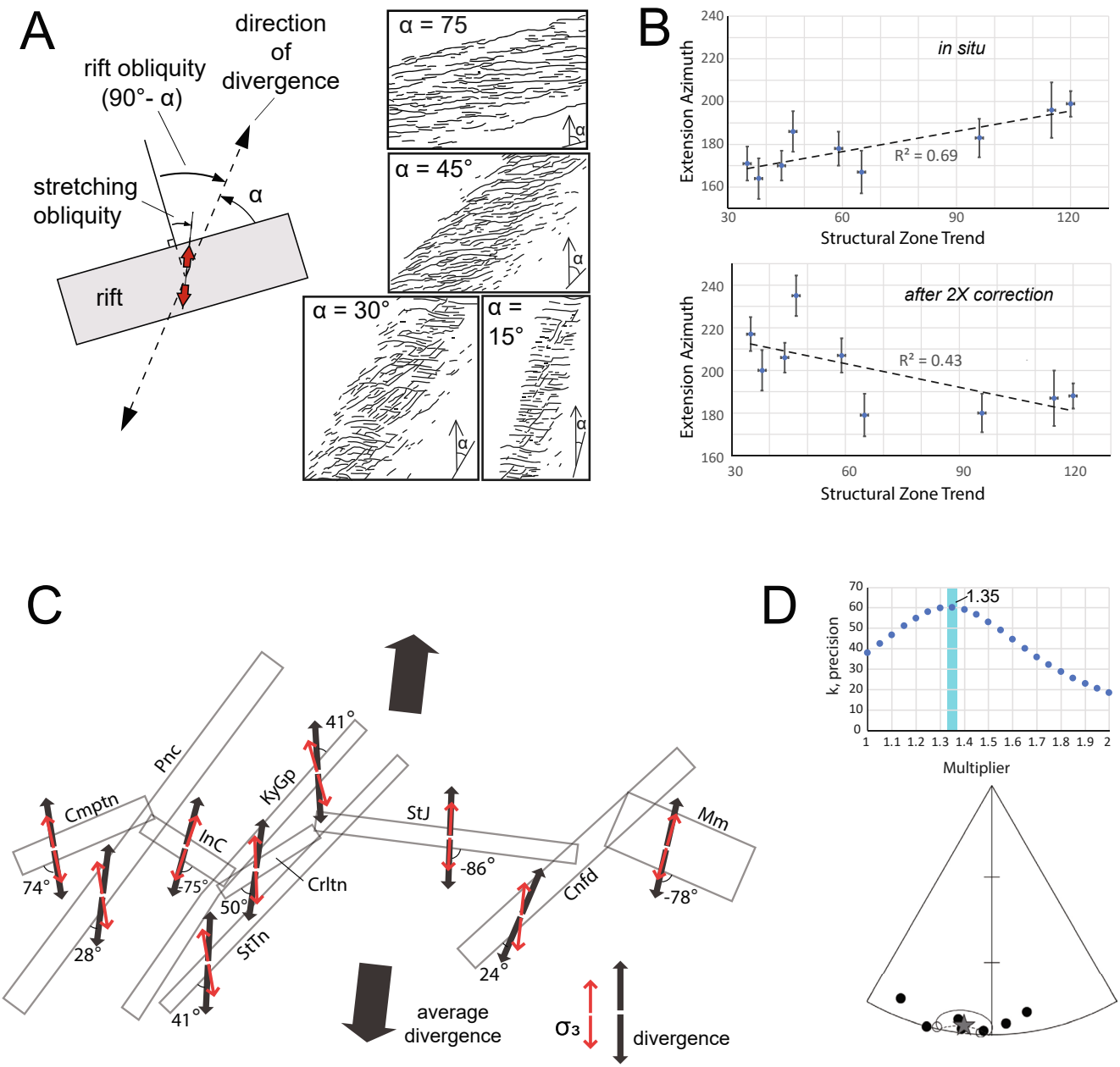

Figure 14. Comparison of fault-slip results to oblique rift models and stress refraction estimates. (a) Oblique rift model (from Withjack & Jamison, 1986) and examples of fault trace maps for different obliquity experiments in clay models, adapted from Clifton et al. (2000). (b) Correlations between internal extension axes (with 2 sigma error limits) and azimuths for structural zones both in situ (upper) and after theoretical correction (lower) for refraction. (c) Oblique rift model for study area showing trend of tension axes (red arrows) within the different structural zones and subzones. Calculated external divergence directions (black arrows) and associated α angles for oblique rift model of stress refraction. (d) Empirical best-fit model for stress refraction found by incremental correction between in situ and 2X models. Least dispersion at 1.35X factor shown by maximum value for precision parameter, k, with resulting mean azimuth at 187° ± 7° as shown on partial equal area net.

zone is clockwise and statistically distinct from the 171° ± 8° azimuth from the adjacent northeast-trending Ponca zone. A model assumption that a common regional extension direction was responsible for the D2 deformation is supported by evidence of strain transfer among the different zones that indicates their deformation was coeval. Analytical analyses for transtension (Teyssier et al., 1995; Withjack & Jamison, 1986) predict that the rift obliquity (90°-α) angle is twice (2X) the internal extension angle to the rift normal direction (Figure 14a). For the study area a common regional direction for block divergence during flexural extension was first sought by applying this model 2X correction to calculate α angles for each zone. The resulting estimates for external

extension direction from each zone are more dispersed than their internal σ_3 axes, and a correlation, albeit weaker ($R^2 = 0.43$), to structural zone orientation remains because the 2X assumption overcorrects the inferred external extension directions (Text S5 in the Supporting Information S1). If instead the extension directions for the structural zones are progressively corrected between the in situ and 2X end members (Text S5 in the Supporting Information S1), minimum dispersion among the different predicted external directions was achieved at a 1.35X multiplier (Figure 14d), with the resulting mean external divergence direction trending 187° ± 7°. Using this empirical fit, α estimates determined for the individual structural zones have absolute values that vary from 86° to 24° (Figure 14c). These can be used to compare to the fault kinematics expected in rift models with different obliquities. The predominant normal faulting observed in the west-to west-northwest-striking Compton, Indian Creek, St. Joe, and Maumee zones that have high α angles ranging from 72° to 86° as is predicted for low to moderate oblique rift models, and the right-stepping en echelon sense for faults in the Indian Creek and St. Joe zones (Figures 3, 5 and 6) are consistent with an expected sinistral strike-slip component. Despite a moderate α value of 72°, faults within the Compton zone do not show the expected en echelon arrangement at map scale, but their total rake peak frequency is slightly shifted from 90° toward the expected dextral-normal oblique slip sense as predicted for the east-northeast trend of the zone (Figure 11). The northeast-trending zones of Ponca and the subzones of Mill Creek have intermediate to low α values ranging from 50° to 28°, consistent with their observed mix of both normal and strike-slip faults and the left-stepping en echelon sense of their faults that accommodated dextral transtension (Figures 3, 5 and 6). The Confederate zone yielded the lowest α estimate (24°), consistent with observations that strike-slip faults are dominant within this zone. However, we note that its calculated external stretching direction is the most divergent among those for the individual structural zones (Figure 14d, Text S5 in the Supporting Information S1), perhaps due to modest clockwise vertical-axis rotation of rocks containing the faults within the zone of dominantly dextral strike slip shear.

The strong match between the predictions from oblique rift models and the characteristics of D2 deformation in the study area supports the inferences from geophysical data (Text S4 in the Supporting Information S1) and regional summaries that much of the extension within Paleozoic strata was localized above preexisting zones of weakness (Figure 15a) in Mesoproterozoic crystalline basement. The near orthogonal divergence predicted across the St. Joe structural zone ($\alpha = 86°$) suggests that it could have newly broken isotropic crust during flexural extension. However, the right-stepping nature of its internal fault segments and its coincidence with a boundary between areas of low and high magnetization in geophysical data (Text S4 in the Supporting Information S1) indicate it is more likely that this zone followed an optimally oriented preexisting contact or fault zone in the basement. Within the northeast-trending Ponca and Mill Creek zones, dextral transtension was accommodated by both normal and strike-slip fault types (Figure 11), raising the question of whether these different stress states were two subevents in time. However, no consistent field relations were observed that documented different timing between D2 normal and strike-slip faults within these zones and it is inferred that their causative paleostress states were probably overlapping in time rather than being temporally discrete. The mixture of normal and strike-slip faulting in a transtensional setting may have analogy to that for the East California shear zone where earthquake focal mechanisms demonstrate contemporaneous normal and strike-slip faulting (e.g., Lewis, 2007; Lewis et al., 2007) partitioned by depth at an inferred decollement. For the study area, the more frequent observations of strike-slip faults in the stiffer Ordovician and Mississippian carbonates than in overlying Pennsylvanian strata (Figures 8b and 8c) could reflect both depth and rheological partitioning as the greater proportions of shale in Pennsylvanian strata facilitated lateral flowage in shallower stratigraphic levels. Analog experiments by Schlische et al. (2002) demonstrated changes of fault patterns above a buried fault where ductile strata allowed flowage.

Relatively few field studies have been conducted that have used fault-slip analyses to directly test models of oblique rifting (e.g., Bonini et al., 2019; Liu et al., 2019; Umhoefer & Stone, 1996). Compared to the single direction of weakness used in examples like the Gulf of California rift (Bonini et al., 2019; Umhoefer & Stone, 1996), this study has the advantage of being able to use multiple directions of inferred basement weaknesses to independently solve for a common external divergence direction. Moreover, the low extensional strains that affected this foreland setting decrease the potential of complicating factors such as large vertical-axis rotations of fault blocks during transtension (e.g., Bennett & Oskin, 2014) that could have reoriented faults, resulting in biased estimates of paleostress directions. For this study, a smaller refraction of extension directions above the weak zones than predicted by the 2X theoretical values for oblique rifts (Teyssier et al., 1995; Withjack & Jamison, 1986) was indicated by the empirical 1.35X fitting factor. The controls on this difference are uncertain, but perhaps a narrow

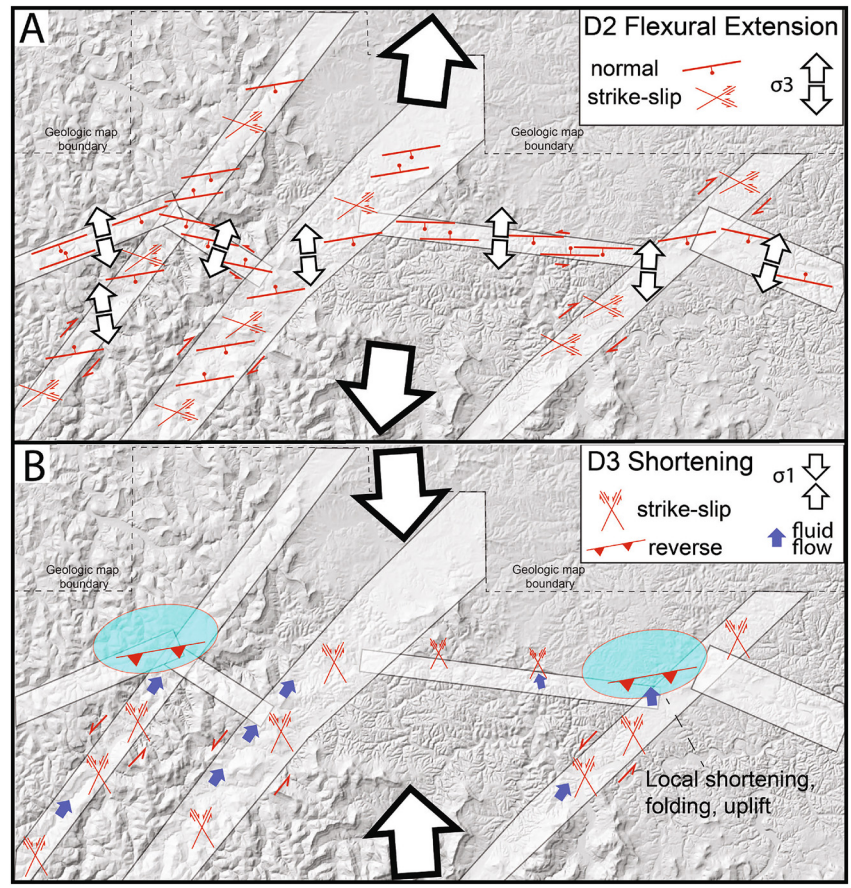

Figure 15. Tectonic models for foreland deformation in study area. (a) Flexural extension of D2 phase by reactivation of preexisting basement weaknesses at varying angles of obliquity, leading to stress refractions and varying proportions of normal and strike-slip faults. (b) North-south shortening of D3 phase leading to strike-slip reactivation of northeast-trending zones, localized incipient inversion at block corners, and structurally controlled mineralizing fluid flow.

breadth of basement fault zones that underlie the study area contrast with the lithospheric scale of weaknesses that have been invoked for most oblique rift models.

5.1.2. Age Constraints and Setting Within Foreland Basin System

Both the similarity of normal faults in the southern Ozarks to those in the Arkoma basin and the available timing constraints for structures from the study area support prior conclusions (Arbenz, 1989; Bradley & Kidd, 1991; Hudson, 2000) that north-south extension that affected the southern flank of the Ozark dome was caused by flexure of the Laurentian continental margin ahead of the advancing Ouachita orogenic belt in a peripheral foreland basin system (DeCelles, 2012). In the study area, there is no evidence of normal growth faulting in the preserved Pennsylvanian strata and thus D2 faults are younger than the youngest lower Atokan strata that cap the ridges. Normal faults farther south in the western Arkoma basin (Arbenz, 1989; Buchanan & Johnson, 1968) began slip contemporaneous with sedimentation of middle Atokan sediments (Houseknecht, 1986; Zachry & Sutherland, 1984). If extension was synchronous in the study area and the Arkoma basin, this would suggest development of D2 structures in middle Atokan. However, extension might be expected to young toward the craton if it tracked inward migration of a lithospheric flexural wave (DeCelles, 2012) ahead of Ouachita belt accretion. An end of D2 extension in the study area is constrained from field relations (Figure 9) that demonstrate it was overprinted by D3 shortening that most likely resulted from propagation of compressional stresses into the craton as the Ouachita accretionary belt advanced onto the continental margin. Within the Arkoma basin to the south, the north-south shortening was active at least past the youngest preserved Desmoinesian strata that are folded (Hendricks & Park, 1950) and likely lasted into Late Pennsylvanian to early Permian (Denison, 1989; Viele & Thomas, 1989).

Considered in the framework of flexural foreland systems (DeCelles, 2012), available evidence from thermal maturity and regional stratigraphy suggests that D2 extension in the study area occurred in distal foredeep or proximal forebulge settings. Whereas the D2 extension in the study area and normal growth faults in the foreland Arkoma basin share a similar genetic relationship to flexure of the foreland, constraints on thermal maturity indicates that the study area was never as deeply buried as even younger strata preserved in the Arkoma basin (Houseknecht & Matthews, 1985). Low thermal maturation of rocks within the study area is shown by conodont color alteration indices of 1.5 from the most deeply exposed Ordovician rocks (Hudson et al., 2006) and a lignite grade of coal seams within lower Pennsylvanian strata compared to the high bituminous to semi-anthracite coal grades for Desmoinesean strata of the Arkoma basin to the south (Haley, 1982). A northward onlap of basal sandstones of the Atoka Formation in the southern Ozarks region (McGilvery et al., 2016; Shinn, 1979) match predictions for distal foredeep to proximal forebulge settings (DeCelles & Giles, 1996). DeCelles (2012) noted that onset of flexural uplift produces tensional fiber stresses in the forebulge regions that break the upper crust along minor but potentially numerous normal faults, which may be controlled by preexisting weaknesses.

5.2. North-South Shortening and Incipient Inversion

Whereas flexural extension was dominant across the study area, the fault slip analyses demonstrate that the area was overprinted by a more spatially limited D3 phase of north-south shortening. The D3 phase is interpreted to record the migration of shortening from the Ouachita orogeny into the foreland in its later stages (Chinn & Konig, 1973; Craddock & van der Pjium, 1989; Cox, 2009), a process that has been suggested to have acted at a continental scale during late stages of the combined Alleghenany-Ouachita orogenies (Craddock & van der Pjium, 1989; Craddock et al., 1993; Craddock et al., 2017). In addition to the inverted fault-slip tensors presented here, north-south compression is also recorded by a pervasive north-northwest trending joint set in the study area (Hudson et al., 2011) as well as calcite-twin strain analyses (Chinn & Konig, 1973; Craddock & van der Pluijm, 1989; Craddock et al., 1993) and other fracture analyses (Cox, 2009) from the southern Ozarks region. North-south shortening in the study area resulted in newly formed, steeply dipping strike-slip faults (Figure 9) that have strongest strike modes of north-northeast and northwest (Figure 10c). Less frequent northeast and west-northwest strike modes for the D3 strike-slip faults likely represent reactivated faults of similar trends from the older D2 fault population (compare to Figure 10b). Spatially, most of the D3 strike-slip faults are concentrated within the northeast-trending Ponca, Mill Creek and Confederate structural zones (Figure 12). Because these zones are thought to overlie basement structures that were active during D2 dextral transtension, it is likely that the slip-sense across the basement structures was reversed during D3 compression to accommodate a sinistral slip component (Figure 15b).

Documented reverse faults that record north-south shortening in the study area are comparatively rare (Figure 13) and accommodated only small strains, yet their presence may be important because they may suggest localized incipient inversion of previous extensional structures. Eastern and western subareas, respectively, are found in the immediate footwall of the St. Joe normal fault or the combined Compton and California Point normal faults and in both areas the footwalls contain locally developed anticlines (Figures 5a and 4d). Both subareas are located at the corners of crustal blocks bounded by the normal faults and intersecting northeast-trending structural zones (Figure 15b). The western subarea of the Sneeds Creek dome developed adjacent to intersections of the Compton and Indian Peak normal fault zones with the northeast trending Ponca zone. The eastern subarea of reverse faulting occurs adjacent to the intersection of the St. Joe zone with the northeast-trending Confederate zone. These spatial relationships suggest, under the influence of a shallowly plunging, north-south trending σ_1 axis, that stress concentrations at block corners drove local shortening accommodated by reverse faulting and folding in the footwall of normal faults (Figure 15b). In this setting it is speculated that the σ_3 axis was flipped to subvertical from its subhorizontal inclination within the sinistrally reactivated northeast-trending zones.

Inversion of slip along normal faults in former extensional terranes has been documented in many areas around the world (Bonini et al., 2012; Buchanan & Buchanan, 1995; Coward, 1994) like the North Sea (McClay, 1995), southeastern Asia (Morley et al., 2007), and Africa (Beauchamp et al., 1996), but typically it is detected in more advanced stages where reverse offset can be proven at some preserved stratigraphic level along former normal faults. In the study area, only normal offset along the map-scale faults is preserved (Figures 7b and 7f) and it is likely that these areas represent an incipient stage of development compared to most recognized inversion examples. Nonetheless, the development of small-scale reverse faulting and anticlines in the immediate footwall

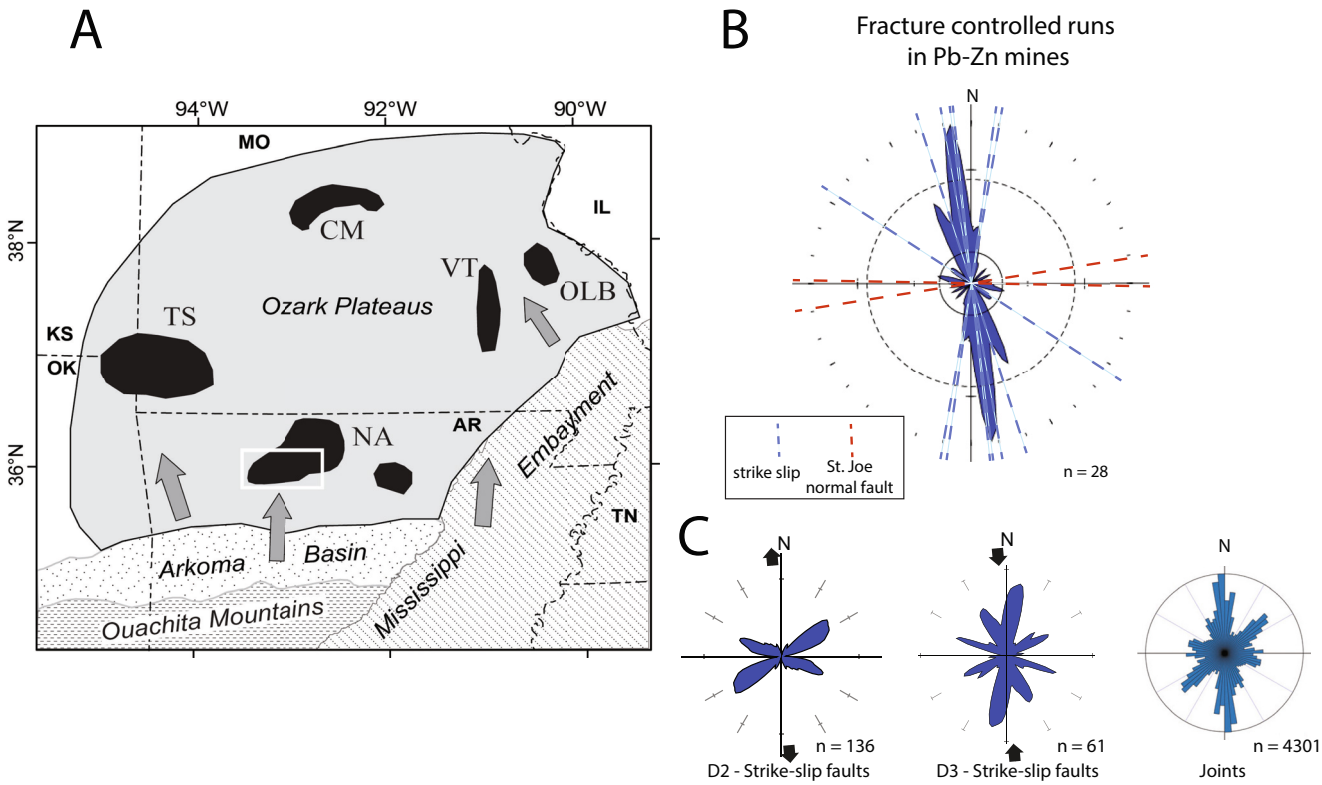

Figure 16. Comparison between mineralized fractures and fractures from D2 and D3 deformation episodes. (a) Physiographic provinces and lead-zinc districts (black areas) of the Ozark Plateaus region. Gray arrows represent proposed paths of fluid flow from the foreland basin areas (from Leach, 1994). White box is study area. Lead-zinc mining districts are CM – Central Missouri, NA – Northern Arkansas, OLB – Old Lead Belt, TS – Tri-State, and VT – Viburnum Trend. (b) Rose diagram of strikes of mineralized fractures and faults from the southwestern part of the Northern Arkansas (NA) district as reported by McKnight (1935). Dashed lines are trends of individual strike-slip (blue) and normal (red) fault-controlled zones. (c) Comparative rose diagrams of strikes of D2 strike-slip faults, D3 strike-slip faults, and joints (Hudson et al., 2011) from the study area.

of these faults (Figures 5a, 6b and 7b) is similar to the setting of cutoff thrusts and growth anticlines in the footwalls of other steeply dipping normal faults affected by inversion (McClay, 1995; Powell, 1989). The bridging of compressional deformation into the footwall of the normal faults may be due to their steep dip, which is unfavorable for reactivation in the absence of high fluid pressures (Sibson, 1995). In the study area, a focusing of fluid flow during D3 deformation (discussed next) may have aided localization of the incipient inversion.

5.3. Relations Between Faulting and Regional Brine Flow

Compression within the Arkoma basin and growth of topographic head in the Ouachita fold and thrust belt is recognized to have driven regional scale fluid flow into broad foreland areas of the Laurentian midcontinent in response to the collision with Gondwana (Appold & Nunn, 2005; Bethke & Marshak, 1990; Clendenin & Duane, 1990; Lewchuk & Symons, 1995). Temperature estimates derived from fluid inclusions associated with Mississippi Valley type (MVT) mineralization record the passage of warm basinal brines through sedimentary aquifers within the Ozark dome (Leach & Rowan, 1996). Late Pennsylvanian to early Permian ages estimated for MVT mineralization from paleomagnetic (Lewchuk & Symons, 1995; Pan et al., 1990) and isotopic studies (Brannon et al., 1996) support linking regional fluid flow to the Ouachita orogeny (Leach et al., 2001). Whether MVT mineralization was associated with D2 extensional versus D3 compressional faulting (Leach et al., 2001), and whether fluid flow facilitated reactivation of preexisting structures (Cox, 2009), are valid questions.

The Buffalo River study area overlaps the southwestern part (Figure 16a) of the Northern Arkansas lead-zinc mineral district (McKnight, 1935) where MVT mineralization was hosted in the Ordovician Everton Formation and Mississippian Boone Formation. Both horizons are stratigraphically higher than larger MVT deposits hosted in Cambrian strata in southeastern Missouri (Leach, 1994). These stratigraphic associations coupled with mine

locations within or close to structural zones in the study area (Figure 12), suggest that fracture permeability from faulting facilitated the rise of mineralizing brines from deeper levels in the Northern Arkansas district (Erikson et al., 1988; Hudson, 2000), similar to what has been inferred for the Tri-State district (Appold & Nunn, 2005). From his onsite inspections or discussions with mine operators, McKnight (1935) described the orientations of numerous elongate mineralization "runs" guided by fractures or small faults at many mines in the district (Text S6 in the Supporting Information S1). A dominance of north-northwest to north-northeast strikes for the mineralized runs (Figure 16b), many following small faults with horizontal striations (McKnight, 1935), indicates that mineralization followed strike-slip faults or associated north-south striking extensional joints that developed during D3 compression. Support for coeval infiltration of brine and D3 faulting during north-south compression also comes from the observations of this study that silicification, a common early stage of MVT paragenesis (McKnight, 1935; Leach et al., 1975), was preferentially localized at several field sites where D3 faulting overprints the more widespread D2 faults (Figures 8 and 11). Evidence suggesting that older D2 extensional structures provided important fracture permeability pathways for MVT brines is demonstrated by the localization of ore in fault breccias along the St. Joe normal fault (e.g., Figure S6-1a in the Supporting Information S1) at the Spier and Big Hurricane mines (McKnight, 1935). These field relations allow that brine migration could have begun earlier, during D2 extension. However, the presence of D3 strike-slip faults adjacent to the Big Hurricane mine in the footwall of the St. Joe fault (Figure S6-1b in Supporting Information S1) suggests that high fluid pressures may have facilitated this D3 faulting and that the associated mineralization was later. Father east, mineralization at the Excelsior mine (Figure 12) followed a small fault that parallels and lies in the footwall of the St. Joe fault (McKnight, 1935). This mineralization zone coincides with the eastern subarea of observed reverse faulting and folding and both the MVT mineralization and the inferred area of incipient inversion (Figures 6b, 11 and 14b) lie within a larger but still restricted area of strong silicification encompassing sites of silicified collapse breccias and precipitation of quartz crystals in vugs and veins (Hudson & Turner, 2009). Such spatial correlations between MVT mineralization, silicification, and localized areas of D3 shortening support hypotheses that high fluid pressures from brine flow may have facilitated reactivation of the preexisting fault zones in the Ozarks region (Cox, 2009) and also fit rock mechanical requirements that the reactivation of steeply dipping normal faults under horizontal compression typically require fluid pressures above hydrostatic (e.g., Sibson, 1985, 1995; Turner & Williams, 2004).

From these relations, we conclude that the regional flow of mineralized brines probably began after the main episode of Middle Pennsylvanian flexural extension (D2) and was guided by the increased fracture permeability of such structures facilitating rise to shallow levels within the Northern Arkansas MVT district. Brine flow was most likely contemporary with the change to north-south compression (D3) and may have aided inversion of preexisting structures. Regional MVT mineralization associated with migration of north-south compressive stresses into the foreland is consistent with models for fluid flow being driven from the growing Ouachita orogen either due to topographic head or by pressure driven expulsion of the fluids during the Late Pennsylvanian to early Permian (Bethke & Marshak, 1990; Leach et al., 2001; Oliver, 1986).

6. Summary

Faults and folds in a foreland area on the southern flank of the Ozark dome record phases of widespread D2 north-south flexural extension and more spatially limited D3 north-south compression that developed in response to progressive encroachment of the late Paleozoic Ouachita orogenic belt from to the south. The distribution of map-scale structures and an analysis of fault-slip data collected systematically during geologic mapping in the Buffalo River watershed study area demonstrate that most deformation was focused in several linear zones between largely undeformed areas. Comparisons to the style and timing of normal faulting in the Arkoma basin to the south suggests that the D2 extension occurred in a distal foredeep to proximal forebulge setting as the southern margin of Laurentia was flexed beneath a growing thrust load of the Ouachita belt during Middle Pennsylvanian. D2 extension was concentrated in structural zones having sets of discontinuous, often en echelon normal and strike-slip faults and linking monoclinal folds whose northeast and west-northwest trends are similar to basement weaknesses that have been recognized throughout the midcontinent. That these structural zones reactivated underlying basement weaknesses is supported by their close match to the predictions of oblique rift models (with α values ranging between 86° and 24°) in which both the proportions of normal and strike-slip faulting and the internal extension directions vary with orientation of the zones. An empirical correction for stress

deflection within the differently oriented structural zones yields an external divergence direction of 187°± 7°, with a tightest fit achieved using a 1.35X rather than a theoretical 2X multiplier factor between the rift normal and internal stretching direction angles.

Propagation of north-south Ouachita shortening into the foreland caused growth of small strike-slip and sparse reverse faults of a D3 phase that overprinted older D2 extensional structures. Strike-slip faults were predominant during D3 shortening and were concentrated in reactivated northeast-trending structural zones. Two areas where reverse faults and local anticlines developed in the footwalls of older normal faults are both near intersections of northeast- and west-northwest-trending structural zones and are interpreted as areas of incipient inversion caused by stress concentrations at fault-block corners. Spatial correlations between areas of north-south shortening and paleofluid flux marked by silicification or lead-zinc mineralization as well as the orientation of structurally controlled mineralization runs indicate that regional fluid flow of MVT brines was coeval with and may have enhanced inversion during Late Pennsylvanian to early Permian.

Data Availability Statement

All data supporting the interpretations and conclusions of this study can be found in the manuscript text, figures, and the supporting information file, and all fault data used in this report are available at Hudson and Turner, 2022 (https://doi.org/10.5066/P92TLPU2).

Acknowledgments
Data presented in this report were collected while conducting geologic mapping funded by the U.S. Geological Survey National Cooperative Geologic Mapping Program and by external grants from the National Park Service, support the authors gratefully acknowledge. The authors thank A. Chandler, S. Ausbrooks, and R. Hutto of the Arkansas Geological Survey for sharing helpful discussions about the study area as well as locations of several fault sites that were examined. Discussions on fault-slip analyses with S.A. Minor and J.S. Caine and on geophysical surveys with A. McCafferty are greatly appreciated. R.Cox has provided important discussion on the broader development of the Ozark Plateaus area through the years. This report benefitted from helpful review comments from R. Cox, S. Marshak, J. Lund-Snee, J. Craddock, and M. Rusmore. Paleostress inversions were conducted using Pangea Scientific MyFault (ver. 1.05) software. Any use of trade, firm, or product names is for descriptive purposes only and does not imply endorsement by the U.S. Government.

References

Anderson, E. M. (1951). *The dynamics of faulting and dyke formation with applications to Britain* (2nd ed.), Edinburgh: Oliver and Boyd.

Angelier, J. (1984). Tectonic analysis of fault slip data sets. *Journal of Geophysical Research*, *89* (B7), 5835–5848. https://doi.org/10.1029/jb089ib07p05835

Angelier, J. (1990). Inversion of field data in fault tectonics to obtain the regional stress-III, A new rapid direct inversion method by analytical means. *Geophysical Journal International*, *103*, 363–376.

Appold, M. S., & Nunn, J. A. (2005). Hydrology of the western Arkoma basin and Ozark platform during the Ouachita orogeny: Implications for Mississippi Valley-type ore formation in the tri-state Pb-Zn district. *Geofluids*, *5*, 308–325. https://doi.org/10.1111/j.1468-8123.2005.00122.x

Arbenz, J. K. (1989). Ouachita thrust belt and Arkoma basin. In R. D. Hatcher,Jr., W. A. Thomas, & G. W. Viele (Eds.), *The Geology of North America*, F-2: The Appalachian-Ouachita orogen in the United States (621–634 pp). Boulder, CO: Geological Society of America.

Arbenz, J. K. (2008). Structural framework of the Ouachita Mountains. In N. H. Suneson (Ed.), *Stratigraphic and structural evolution of the Ouachita Mountains and Arkoma basin, southeastern Oklahoma and west-central Arkansas: Applications to Petroleum exploration: 2004 field symposium, circular 112A* (pp. 1–40). Norman, OK: Oklahoma Geological Survey.

Aydin, A., & Johnson, A. M. (1978). Development of faults as zone of deformation bands and as slip surfaces in sandstone. *Pure and Applied Geophysics*, *116*, 931–942. https://doi.org/10.1007/bf00876547

Beauchamp, W., Barazangi, M., Demnati, A., & Alji, M. E. (1996). Intracontinental rifting and inversion: Missour Basin and Atlas Mountains, Morocco. *American Association of Petroleum Geologist Bulletin*, *80*, 1459–1482.

Bennett, S. E. K., & Oskin, M. E. (2014). Oblique rifting ruptures continents: Examples from the Gulf of California shear zone. *Geology*, *42*, 215–218. https://doi.org/10.1130/G34904.1

Bethke, C. M., & Marshak, S. (1990). Brine migrations across North America – The plate tectonics of groundwater. *Annual Review of Earth and Planetary Sciences*, *18*, 287–315.

Bonini, M., Cerca, M., Moratti, G., López-Martínez, M., Corti, G., & Gracia-Marroquín, D. (2019). Strain partitioning in highly oblique rift settings: Inferences from the southwestern margin of the Gulf of California (Baja California Sur, México). *Tectonics*, 38. https://doi.org/10.1029/2019TC005566

Bonini, M., Sani, F., & Antonielli, B. (2012). Basin inversion and contractional reactivation of inherited normal faults: A review based on previous and new experimental models. *Tectonophysics*, *522–523*, 55–88. https://doi.org/10.1016/j.tecto.2011.11.014

Bradley, D. C., & Kidd, W. S. F. (1991). Flexural extension of the upper continental crust in collisional foredeeps. *The Geological Society of America Bulletin*, *103*, 1416–1438.

Brannon, J. C., Podosek, F. A., & Cole, S. C. (1996). Radiometric dating of Mississippi Valley–type ore deposits. In D. F. Sangster (Ed.), *Carbonate hosted lead-zinc deposits*, Special publication (Vol. 4, pp. 536–545). Littleton, CO: Society of Economic Geologists.

Buchanan, J. G., & Buchanan, P. G. (Eds.), (1995). *Basin inversion. Geological Society Special Publication* (Vol. 88, pp. 596). London: Geological Society.

Buchanan, R. S., & Johnson, F. K. (1968). Bonanza gas field – A model for Arkoma basin growth faulting. In L. M. Cline (Ed.), *Geology of the western Arkoma basin and Ouachita Mountains, Oklahoma* (pp. 75–85). Oklahoma City, OK: Oklahoma City Geological Society.

Celerier, B., Etchecopar, A., Bergerat, F., Vergely, P., Arthaud, F., & Larent, P. (2012). Inferring stress from faulting: From early concepts to inverse methods. *Tectonophysics*, *581*, 206–219.

Chandler, A. K., & Ausbrooks, S. M. (2003). *Geologic map of the Parthenon quadrangle, Newton county, Arkansas* (map DGM-AR-00680) scale 1:24,000. Little Rock, AR: Arkansas Geological Survey.

Chandler, A. K., & Ausbrooks, S. M. (2015a). *Geologic map of the Eula quadrangle, Newton and searcy counties, Arkansas* (map DGM-AR-00269) scale 1:24,000. Little Rock, AR: Arkansas Geological Survey.

Chandler, A. K., & Ausbrooks, S. M. (2015b). *Geologic map of the Mt. Judea quadrangle, Newton county, Arkansas* (map DGM-AR-00590) scale 1:24,000. Little Rock, AR: Arkansas Geological Survey.

Chandler, A. K., & Ausbrooks, S. M. (2015c). *Geologic map of the Snowball quadrangle, searcy county, Arkansas* (map DGM-AR-00800) scale 1:24,000. Little Rock, AR: Arkansas Geological Survey.

Chinn, A. A., & Konig, R. H. (1973). Stress inferred from calcite twin lamellae in relation to regional structure of northwest Arkansas. *The Geological Society of America Bulletin*, *84*, 3731–3736.
Clendenin, C. W., & Duane, M. J. (1990). Focused fluid flow and Ozark Mississippi Valley-type deposits. *Geology*, *18*, 116–119.
Clifton, A. E., Schlische, R. W., Withjack, M. O., & Ackerman, R. V. (2000). Influence of rift obliquity on fault-population statistics: Results of experimental clay models. *Journal of Structural Geology*, *22*, 1491–1509.
Coward, M. P. (1994). Inversion tectonics. In P. L. Hancock (Ed.), *Continental deformation* (pp. 280–304). Oxford: Pergamon Press.
Cox, R. T. (2009). Ouachita, appalachian, and ancestral rockies deformations recorded in mesoscale structures on the foreland Ozark plateaus. *Tectonophysics*, *474*, 674–683. https://doi.org/10.1016/j.tecto.2009.05.005
Craddock, J. P., Jackson, M., Van der Pluijm, B. A., & Versical, R. T. (1993). Regional shortening fabrics in eastern North America: Far-field stress transmission from the Applachian-Ouachita orogenic belt. *Tectonics*, *12*, 257–264.
Craddock, J. P., Malone, D. H., Porter, R., Compton, J., Luczaj, J., Konstantinou, A., et al. (2017). Paleozoic reactivation structures in the Appalachian-Ouachita-Marathon foreland: Far-field deformation across Pangea. *Earth-Science Reviews*, *169*, 1–34.
Craddock, J. P., & Van der Pluijm, B. A. (1989). Late Paleozoic deformation of the cratonic carbonate cover of eastern North America. *Geology*, *17*, 416–419.
Croneis, C. (1930). *Geology of the Arkansas paleozoic Area with especial reference to oil and gas possibilities* (Bulletin 3, pp. 457). Little rock, AR: *Arkansas geological survey*.
Cruden, D. M., & Charlesworth, H. A. K. (1976). Errors in strike and dip measurements. *The Geological Society of America Bulletin*, *87*, 977–980.
Davis, G. H. (1999). *Structural geology of the Colorado plateau region of Southern Utah, with special emphasis on deformation bands* (Vol. 342, pp. 1–155). Boulder, CO: Geological Society of America Special Paper.
DeCelles, P. G. (2012). Foreland basin systems revisited: Variations in response to tectonic settings. In C. Busby & A. A. Perez (Eds.), *Tectonics of sedimentary basins: Recent advances* (pp. 405–426). Blackwell.
DeCelles, P. G., & Giles, K. A. (1996). Foreland basin systems. *Basin Research*, *8*, 105–123.
Denison, R. E. (1989). Foreland structure adjacent to the Ouachita foldbelt. In R. D. Hatcher,Jr., W. A. Thomas, & G. W. Viele (Eds.), *The geology of North America* (Vol. F-2). *The Appalachian-Ouachita orogen in the United States* (pp. 681–688). Boulder, CO: Geological Society of America.
Dickinson, W. R., & Lawton, T. F. (2003). Sequential intercontinental suturing as the ultimate control for Pennsylvanian Ancestral Rocky Mountains deformation. *Geology*, *31*, 609–612.
Erickson, R. L., Chazin, B., Erickson, M. S., Mosier, E. L., & Whitney, H. (1988). Tectonic and stratigraphic control of regional subsurface geochemical patterns, midcontinent, U.S.A. In G. Kisvarsanyi & S. K. Grant (Eds.), *Tectonic control of ore deposits and the vertical and horizontal extent of ore systems* (pp. 435–446). Rolla, MO: University of Missouri Press.
Faulds, J. E., & Varga, R. (1998). The role of accommodation zones and transfer zones in the regional segmentation of extended terranes. In J. E. Faulds & J. H. Stewart, (Eds.), *Accommodation zones and transfer zones: The regional segmentation of the Basin and Range province* (Vol. 343, pp. 1–45). Boulder, CO: Geological Society of America Special Paper.
Flawn, P. T., Goldstein, A., King, P. B., & Weaver, C. E. (1961). *The Ouachita System*. 6120, 401. Austin, TX: University of Texas Publication.
Gavin, G., Ge, S., Person, M. A., & Sverjensky, D. A. (1993). Genesis of stratabound ore deposits in the midcontinent basins of the North America! The role of regional groundwater flow. *American Journal of Science*, *293*, 497–568.
Haley, B. (1982). Geology and energy resources of the Arkoma Basin, Oklahoma and Arkansas. *University of Missouri-Rolla UMR Journal*, *3*, 43–53.
Haley, B. R., Glick, E. E., Bush, W. V., Clardy, B. F., Stone, C. G., Woodward, M. B., & Zachry, D. L. (1993). *Geologic map of Arkansas,* scale 1:500,000 (Arkansas geological commission in cooperation with U.S). Little rock, AR: Geological Survey.
Hancock, P. L. (1985). Brittle microtectonics: Principles and practice. *Journal of Structural Geology*, *7*, 437–457.
Hancock, P. L., & Bevan, T. G. (1987). Brittle modes of foreland extension. In M. P. Coward, J. F. Dewey, & P. L. Hancock (Eds.), *Continental extensional tectonics, special publications* (Vol. 28, pp. 127–137). London, Geological Society of London.
Harding, T. P. (1985). Seismic characteristics and identification of negative flower structures, positive flower structures, and positive structural inversion. *American Association of Petroleum Geologists Bulletin*, *69*, 585–600.
Hardy, S., & McClay, K. (1999). Kinematic modelling of extensional fault-propagation folding. *Journal of Structural Geology*, *21*, 695–702.
Hendricks, T. A., & Park, B. (1950). *Geology of the fort smith district* (pp. 67–94). Professional Paper 221-E. Washington, D.C: U.S. Geological Survey.
Hildenbrand, T. G., Griscom, A., Van Schmus, W. R., & Stuart, W. D. (1996). Quantitative investigations of the Missouri gravity low: A possible expression of a large, Late Precambrian batholith intersecting the New Madrid seismic zone. *Journal of Geophysical Research*, *101*, 21921–21942.
Hippolyte, J. C., Bergeret, F., Gordon, M. B., Bellier, O., & Espurt, N. (2012). Keys and pitfalls in mesoscale fault anaylsis and paleostress reconstructions, the use of Angelier's methods. *Tectonophysics*, *518*, 144–162.
Houseknecht, D. W. (1986). Evolution from passive margin to foreland basin: The Atoka Formation of the Arkoma Basin, south-central U.S.A. In P. A. Allen & P. Homewood (Eds.), *Foreland basins, international association of sedimentologists special publication* (Vol. 8, pp. 327–345). Hoboken, NJ: Wiley.
Houseknecht, D. W., & Matthews, S. M. (1985). Thermal maturity of Carboniferous strata, Ouachita Mountains. *American Association of Petroleum Geologists Bulletin*, *69*, 335–345.
Hudson, M. R. (2000). Coordinated strike-slip and normal faulting in the southern Ozark dome of northern Arkansas: Deformation in a late Paleozoic foreland. *Geology*, *28*, 511–514.
Hudson, M. R., & Cox, R. T. (2003). Late Paleozoic tectonics of the southern Ozark dome. In R. T. Cox (Ed.), *Field trip guidebook for joint south-central and southeastern sections*, *Geological Society of America, Tennessee Division of Geology Report of Investigations* (Vol. 51, pp. 15–32). Nashville, TN: Tennessee Geological Survey.
Hudson, M. R., & Murray, K. E. (2003). *Geologic map of the ponca quadrangle, Newton, Boone, and carroll counties, Arkansas* (Miscellaneous field investigations map MF-2412) 1:24,000 scale. Denver, CO: U.S. Geological Survey. Retrieved from http://pubs.usgs.gov/mf/2003/mf-2412
Hudson, M. R., & Murray, K. E. (2004). *Geologic map of the hasty quadrangle, Boone, and Newton counties, Arkansas* (scientific investigations map SIM-2847) 1:24,000 scale. Denver, CO: U.S. Geological Survey. Retrieved from http://pubs.usgs.gov/sim/2004/2847/
Hudson, M. R., Murray, K. E., & Pezzutti, D. (2001). *Geologic map of the jasper quadrangle, newton and boone counties, Arkansas* (Miscellaneous field studies map MF-2356) 1:24,000 scale. Denver, CO: U.S. Geological Survey. Retrieved from http://pubs.usgs.gov/mf/2001/mf-2356

Hudson, M. R., & Turner, K. J. (2007). *Geologic map of the boxley quadrangle, Newton and Madison counties, Arkansas* (scientific investigations map 2991) 1:24,000 scale. Denver, CO: U.S. Geological Survey. Retrieved from http://pubs.usgs.gov/sim/2991/

Hudson, M. R., & Turner, K. J. (2009). *Geologic map of the St. Joe quadrangle, Searcy and marion counties, Arkansas* (scientific investigations map 3074) 1:24,000 scale. Denver, CO: U.S. Geological Survey. Retrieved from http://pubs.usgs.gov/sim/3074/

Hudson, M. R., & Turner, K. J. (2014). *Geologic map of the west-central Buffalo national River region, Arkansas* (scientific investigations map 3314) 1:24,000 scale. Denver, CO: U.S. Geological Survey. Retrieved from http://pubs.usgs.gov/sim/3314/

Hudson, M. R., & Turner, K. J. (2014). Thickness variations of Upper Mississippian strata in the Western Buffalo River region of northern Arkansas: Evidence of Late Mississippian tectonic activity in the southern Ozark Dome. *Geological Society of America Abstracts with Programs*, *46* (1), 3.

Hudson, M. R., & Turner, K. J. (2016). *Geologic map of the murray quadrangle, Newton county, Arkansas* (scientific investigations map 3360) 1:24,000 scale. Denver, CO: U.S. Geological Survey. https://doi.org/10.3133/sim3360

Hudson, M. R., & Turner, K. J. (2022). *Fault data collected between 1996 and 2019 from the Buffalo River watershed area, northern Arkansas*. U.S. Geological Survey data release. https://doi.org/10.5066/P92TLPU2

Hudson, M. R., Turner, K. J., & Bitting, C. (2011). Geology and karst landscapes of the buffalo national river area, northern Arkansas. In E. L. Kuniansky (Ed.), *U.S. Geological survey Karst interest group proceedings, Fayetteville, Arkansas* (pp. 191–212). Scientific investigations report 2011–5031. Denver, CO: U.S. Geological Survey. Retrieved from http://pubs.usgs.gov/sir/2011/5031/

Hudson, M. R., Turner, K. J., & Repetski, J. E. (2006). *Geologic map of the western grove quadrangle, northwestern Arkansas* (Scientific Investigations Map 2921) 1:24,000 scale. Denver, CO: U.S. Geological Survey. Retrieved from http://pubs.usgs.gov/sim/2921/

Lawton, T. F., Blakey, R. C., Stockli, D. F., & Liu, L. (2021). Late Paleozoic (Late Mississippian-Middle Permian) sediment provenance and dispersal in Western equatorial Pangea. *Palaeogeography, Palaeoclimatology, Palaeoecology*, *572*, 110386. https://doi.org/10.1016/j.palaeo.2021.110386

Leach, D. L. (1994). Genesis of the Ozark Mississippi Valley-type metallogenic province, Missouri, Arkansas, Kansas, and Oklahoma, USA. In L. Fontbote & M. Boni (Eds.), *Sediment-hosted Zn–Pb ores* (pp. 104–138). Berlin: Springer-Verlag.

Leach, D. L., Bradley, D., Lewchuk, M. T., Symons, D. T. A., De Marsily, G., & Brannon, J. (2001). Mississippi Valley-type lead-zinc deposits through geological time: Implications from recent age-dating results. *Mineralium Deposita*, *36*, 711–740.

Leach, D. L., Nelson, R. C., & Williams, D. (1975). Fluid inclusion studies in the Northern Arkansas zinc district. *Economic Geology*, *70*, 1084–1091.

Leach, D. L., & Rowen, E. L., (1996). Genetic link between Ouachita foldbelt tectonism and the Mississippi Valley-type lead-zinc deposits of the Ozarks. *Geology*, *14*, 931–935.

Lewchuk, M. T., & Symons, D. T. A. (1995). Age and duration of Mississippi Valley-type oremineralization events. *Geology*, *23*, 233–236.

Lewis, J. C. (2007). Fine-scale partitioning of contemporary strain in the southern Walker Lane: Implications for accommodating diverent strike slip motion. *Journal of Structural Geology*, *29*, 1201–1215.

Lewis, J. C., Twiss, R. J., Pluhar, C. J., & Monastero, F. C. (2007). Multiple constraints on divergent strike-slip deformation along the eastern margin of the Sierran microplate, SE California. In A. B. Till, S. M. Roeske, J. C. Sample, & D. A.Foster (Eds.), *Exhumation associated with continental strike-slip fault systems* (Vol. 434, pp. 107–128). Boulder, CO: Geological Society of America Special Paper. https://doi.org/10.1130/2007.2434(06)

Liu, Y. A., Murphy, M. A., Van Wijk, J., Koning, D. J., Smith, T., & Andrea, R. A. (2019). Progressive opening of the northern Rio Grande rift based on fault structure and kinematics of the Tusus-Abiquiu segment in north-central New Mexico, U.S. *Tectonophysics*, *753*, 15–35.

Marrett, R., & Allmendinger, R. W. (1990). Kinematic analysis of fault–slip data. *Journal of Structural Geology*, *12* (8), 973–986.

Marshak, S., Domrois, S., Albert, C., Larson, T., Pavlis, G., Hamburger, M., et al. (2017). The basement revealed: Tectonic insight from a digital elevation model of the Great Unconformity, USA cratonic platform. *Geology*, *45*, 391–394. https://doi.org/10.1130/G38875.1

Marshak, S., Karlstrom, K., & Timmons, J. M. (2000). Inversion of Proterozoic extensional faults: An explanation for the pattern of Laramide and Ancestral Rockies intracratonic deformation, United States. *Geology*, *28*, 735–738.

Marshak, S., & Paulsen, T. (1996). Midcontinent U.S. fault and fold zones: A legacy of Proterozoic intracratonic extensional tectonism? *Geology*, *24*, 151–154.

McCafferty, A. E., & Brown, P. J. (2020). *Airborne magnetic and radiometric survey over northwest Arkansas, 2019–2020*. U.S. Geological Survey data release. https://doi.org/10.5066/P91O2Y8W

McCafferty, A. E., Phillips, J. D., Hofstra, A. H., & Day, W. C. (2019). Crustal architecture beneath the southern midcontinent (USA) and controls on Mesoproterozoic iron-oxide mineralization from 3D geophysical models. *Ore Geology Reviews*. https://doi.org/10.1016/j.oregeorev.2019.102966

McClay, K. R. (1995). The geometries and kinematics of inverted fault systems: A review of analogue model studies. In J. G. Buchanan & P. G. Buchanan (Eds.), *Basin Inversion* (Vol. 88, pp. 97–118). London: Geological Society Special Publication.

McFarland, J. D., III. (1988). The Paleozoic rocks of the Ponca region, Buffalo National River, Arkansas. In O. T. Hayward (Ed.), *Centennial field trip guide* (Vol. 4, 207–210 pp). Boulder, CO: Geological Society of America.

McFarland, J. D., III. (1998). *Stratigraphic summary of Arkansas* (pp. 38). Little Rock, AR: Arkansas Geological Commission.

McGilvery, T. A., Manger, W. L., & Zachary, D. L. (2016). Summary and guidebook of the depositional and tectonic history of the Carboniferous succession, northwestern Arkansas. *Third Biennial Field Conference*, Fayetteville, AR: American Association of Petroleum Geologists Mid-Continent Section.

McKnight, E. T. (1935). *Zinc and lead deposits of northern Arkansas* (pp. 311). (Bulletin 853). Washington, D.C. U.S. Geological Survey.

Michael, A. (1984). The determination of stress from slip data, faults and folds. *Journal of Geophysical Research*, *89*, 11517–11526.

Miser, H. D. (1954). *Geologic map of Oklahoma*: Scale 1:500,000. U.S. Geological Survey in cooperation with Oklahoma Geological Survey.

Morley, C. K., Gabdi, S., & Seusutthiya, K. (2007). Fault superimposition and linkage resulting from stress changes during rifting: Examples from 3D seismic data, Phitsanulok Basin, Thailand. *Journal of Structural Geology*, *29*, 646–663.

Oliver, J. E. (1986). Fluids expelled tectonically from orogenic belts: Their role in hydrocarbon migration and other geologic phenomena. *Geology*, *14*, 99–102.

Pan, H., Symons, D. T. A., & Sangster, D. F. (1990). Paleomagnetism of the Mississippi Valley–type ores and host rocks in the northern Arkansas and Tri-State districts. *Canadian Journal of Earth Sciences*, *27*, 923–931.

Peacock, D. C. P. (2002). Propagation, interaction and linkage in normal fault systems. *Earth-Science Reviews*, *58*, 121–142.

Peacock, D. C. P., Knipe, R. J., & Sanderson, D. J. (2000). Glossary of normal faults. *Journal of Structural Geology*, *22*, 291–305.

Petit, J. P. (1987). Criteria for the sense of movement on fault surfaces in brittle rocks. *Journal of Structural Geology*, *9*, 597–608.

Powell, C. M. (1989). Structural controls on Palaeozoic basin evolution and inversion in southwest Wales. *Journal of the Geological Society of London*, *146*, 439–446.

Quinlan, G. M., & Beaumont, C. (1984). Appalachian thrusting, lithospheric flexure, and the Paleozoic stratigraphy of the Eastern Interior of North America. *Canadian Journal of Earth Sciences*, *21*, 973–996.
Schlische, R. W., Withjack, M. O., & Eisenstadt, G. (2002). An experimental study of the secondary deformation produced by oblique-slip normal faulting. *American Association of Petroleum Geologists Bulletin*, *86*, 885–906.
Shinn, M. R. (1979). *Structural geology of the Brentwood-St. Paul area, northwest Arkansas* Master Thesis (pp. 99). Fayetteville, AR: University of Arkansas.
Sibson, R. H. (1985). A note on fault reactivation. *Journal of Structural Geology*, *7*, 751–754.
Sibson, R. H. (1995). Selective fault reactivation during basin inversion: Potential for fluid redistribution through fault-valve action. In J. G. Buchanan & P. G. Buchanan (Eds.), *Basin Inversion* (Vol. 88, 3–21 pp). London: Geological Society, Special Publication.
Siebenthal, C. E. (1915). *Origin of the zinc and lead deposits of the Joplin region, Missouri, Kansas, and Oklahoma* (pp. 283). Bulletin 606. Washington, DC: U.S. Geological Society.
Simon, J. L. (2018). Forty years of paleostress analysis: Has it attained maturity? *Journal of Structural Geology*. https://doi.org/10.1016/j.jsg.2018.02.011
Spang, J. H. (1972). Numerical method for dynamic analysis of calcite twin lamellae. *The Geological Society of America Bulletin*, *83* (2), 467–472.
Sperner, B., Ratschbacher, L., & Ott, R. (1993). Fault-striae analysis: A turbo pascal program package for graphical presentation and reduced stress tensor calculation. *Computers & Geosciences*, *19* (9), 1361–1388.
Starbuck, E. A. (2017). *Geologic map of Missouri:* Scale 1:500,000; Missouri Department of Natural Resources, Missouri Geological Survey.
Sutherland, P. K. (1988). Late Mississippian and Pennsylvanian depositional history in the Arkoma basin area, Oklahoma and Arkansas. *The Geological Society of America Bulletin*, *100*, 1787–1802.
Teyssier, C., Tikoff, B., & Markley, M. (1995). Oblique plate motion and continental tectonics. *Geology*, *23*, 447–450.
Thomas, W. A. (1989). The Appalachian-Ouachita orogen beneath the Gulf Coastal Plain between the outcrops in the Appalachian and Ouachita Mountains. In R. D. Hatcher,Jr., W. A. Thomas, & G. W. Viele (Eds.), *The Geology of North America* (Vol. F-2). *The Appalachian-Ouachita orogen in the United States* (pp. 537–553). Boulder, CO: Geological Society of America.
Thomas, W. A. (2004). Genetic relationship of rift-stage crustal structure, terrane accretion, and foreland tectonics along the southern Appalachian-Ouachita orogen. *Journal of Geodynamics*, *37*, 549–563.
Thomas, W. A., (2006). Tectonic inheritance at a continental margin. *Geological Society of America Today*, *16* (2), 4–11. https://doi.org/10.1130/1052-5173(2006)016<4:TIAACM>2.0.CO;2
Thomas, W. A., Gehrels, G. E., Sundell, K. E., & Romero, M. C. (2021). Detrital-zircon analysis, provenance, and late Paleozoic sediment dispersal in the context of tectonic evolution of the Ouachita orogen. *Geophere*, *17*. https://doi.org/10.1130/GES02288.1
Threet, R. L. (1973). Classification of translations fault slip. *The Geological Society of America Bulletin*, *84*, 1825–1828.
Tron, V., & Brun, J. P. (1991). Experiments on oblique rifting in brittle-ductile systems. *Tectonophysics*, *188*, 71–84.
Turner, J. P., & Williams, G. A. (2004). Sedimentary basin inversion and intra-plate shortening. *Earth-Science Reviews*, *65*, 277–304. https://doi.org/10.1016/j.earscirev.2003.10.002
Turner, K. J., & Hudson, M. R. (2010). *Geologic map of the Maumee quadrangle, Marion and searcy counties, Arkansas* (Scientific Investigations Map 3134) 1:24,000 scale. Denver, CO: U.S. Geological Survey. Retrieved from http://pubs.usgs.gov/sim/3134/
Turner, K. J., & Hudson, M. R. (2018). *Geologic map of the osage SW quadrangle, Newton, Madison, and Carroll counties, Arkansas* (Scientific Investigations Map 3416) 1:24,000 scale. Denver, CO: U.S. Geological Survey. Retrieved from https://doi.gov.org/10.3133/sim3416
Umhoefer, P. J., & Stone, K. A. (1996). Description and kinematics of the SE Loreto basin fault array, Baja California Sur, Mexico: A positive field test of oblique-rift models. *Journal of Structural Geology*, *18*, 595–614.
Van Schmus, W. R., Bickford, M. E., & Turek, A. (1996). Proterozoic geology of the east-central midcontinent basement. In B.van der Pluijm & P. A. Catacosinos (Eds.), *Basement and basins of eastern North America* (Vol. 308, pp. 7–31). Boulder, CO: Geological Society of America Special Paper.
Viele, G. W., & Thomas, W. A. (1989). Tectonic synthesis of the Ouachita orogenic belt. In R. D. Hatcher,Jr., W. A. Thomas, & G. W. Viele (Eds.), *The geology of north America, Vol. F-2. The appalachian-ouachita orogen in the United States* (pp. 695–728). Boulder, CO: Geological Society of America.
Waschbusch, J., & Royden, L. H. (1992). Spatial and temporal evolution of foredeep basins: Lateral strength variations and inelastic yielding in continental lithosphere. *Basin Research*, *4*, 179–196.
Whitmeyer, S. J., & Karlstrom, K. E. (2007). Tectonic model for the Proterozoic growth of North America. *Geosphere*, *3* (4), 220–259. https://doi.org/10.1130/GES00055.1
Wickham, J., Roeder, D. R., & Briggs, G. (1976). Plate tectonic models for the Ouachita foldbelt. *Geology*, *4*, 173–176.
Withjack, M. O., & Jamison, W. R. (1986). Deformation produced by oblique rifting. *Tectonophysics*, *126*, 99–124.
Withjack, M. O., Olsen, J., & Peterson, E. (1990). Experimental models of extensional forced folds. *American Association of Petroleum Geologists Bulletin*, *74*, 1038–1054.
Zachry, D. L., & Sutherland, P. K. (1984). Stratigraphy and depositional framework of the Atoka Formation (Pennsylvanian) Arkoma basin of Arkansas and Oklahoma. In P. K. Sutherland & W. Manger (Eds.), *The Atokan Series (Pennslyvanian) and its Boundaries – A Symposium* (pp. 9–18). Bulletin 136 Norman, OK: Oklahoma Geological Survey.

References From the Supporting Information

Fisher, R. A. (1953). Dispersion on a sphere. *Royal Society of London Proceedings (Series A)*, *217*, 295–305.
Twiss, R. J., Protzman, G. M., & Hurst, S. D. (1991). Theory of slickenline patterns based on the velocity gradient tensor and microrotation. *Tectonophysics*, *186*, 215–239.